カレイ目アキルス科魚類の淡水進出における栄養学的適応機構の解明：脂肪酸代謝酵素系の多様化によるDHA合成能獲得への収斂進化

博士学位論文

カレイ目アキルス科魚類の淡水進出における栄養学的適応機構の解明：脂肪酸代謝酵素系の多様化によるDHA 合成能獲得への収斂進化

2020 年度

（2021 年 3 月）

東京海洋大学大学院

海洋科学技術研究科

応用生命科学専攻

松下　芳之

博士学位論文

カレイ目アキルス科魚類の淡水進出における栄養学的適応機構の解明：脂肪酸代謝酵素系の多様化によるDHA 合成能獲得への収斂進化

2020 年度

（2021 年 3 月）

東京海洋大学大学院

海洋科学技術研究科

応用生命科学専攻

松下　芳之

目次

要旨

長鎖多価不飽和脂肪酸の一種であるドコサヘキサエン酸（DHA; 22:6n-3）は、細胞膜の構成成分として脳や網膜をはじめとする神経組織の発達や維持に関わるほか、神経保護に関与するシグナル分子群であるドコサノイドの前駆体になる等、種々の代替不可能な生理活性を示す。脊椎動物において、DHA は植物等に由来するα-リノレン酸（ALA; 18:3n-3）を起点とし、炭素鎖へ二重結合を導入する不飽和化反応を触媒する不飽和化酵素と、炭素鎖を延長する鎖長延長反応の律速酵素である鎖長延長酵素が関与する DHA 合成経路によって合成される。しかし、多くの海産魚はこれらの脂肪酸代謝酵素の活性を一部欠損しているため DHA を自ら合成できず、海洋環境の餌生物中に豊富に含まれる DHA を直接摂取することが不可欠である。ところが、このような海産魚のうち一部の系統は、DHA の大量生産者が存在せず、餌生物に含まれる DHA が非常に乏しい淡水環境へ進出している。海産養殖魚種における栄養学的研究から、DHA の欠乏は種苗の生残率の低下や発生異常、成長不全を招くことが明らかになっており、淡水へと進出した海産魚系統は、低張環境から体液浸透圧の恒常性を守る生理学的適応のほかに、貧 DHA 環境で生存するための栄養学的適応を果たしているものと予想された。そこで本研究では、南北アメリカ大陸の東岸を中心に海洋から淡水まで幅広く分布するカレイ目のアキルス科魚類に注目し、生息環境の異なる 4 種、すなわち、海産種 *Gymnachirus melas*、降河回遊種 *Trinectes maculatus*、そして淡水産の 2 種 *Apionichthys finis* と *Hypoclinemus mentalis* を材料に用いて、本系統がどのように貧 DHA という栄養学的障壁を克服し、淡水環境に適応したのか明らかにすることを目的とした。

はじめに、降河回遊種 *T. maculatus* を除く、生態学的情報に乏しいアキルス科 3 種について、彼らが実際に経験してきた生息環境を明らかにするため、耳石中のス

トロンチウム（Sr）濃度分布に基づく回遊履歴の推定を行った。その結果、海産種 *G. melas* では、耳石の核を含む中心部と外縁部に近い領域で高く、その中間帯ではやや低い Sr 濃度を示したことから、本種は他の沿岸性カレイ目魚類と同様、河口付近を養育場として利用するものの、海に依存した生活史をもつと考えられた。一方、淡水産の 2 種 *A. finis* と *H. mentalis* では、一貫して低い Sr 濃度を示したことから、彼らは淡水で生活史を完結し、海の餌生物に全く依存していないことが強く示唆された。

次に、アキルス科における淡水進出が系統分化のどの時点で生じたのかについて明らかにするため、16S rRNA 遺伝子の塩基配列に基づく分子系統解析を行った。その結果、アキルス科においては海産系統の *Gymnachirus* 属が最も早く分岐し、次いで降河回遊種を擁する *Trinectes* 属、そして淡水系統の *Apionichthys* 属と *Hypoclinemus* 属が分岐したことが明らかになり、本科は海に起源をもち、系統の分化と共に淡水へ進出したこと、そして海産種 *G. melas* は淡水進出に関わる形質について、祖先的な状態を留めていることが推測された。

続いて、アキルス科 4 種の DHA 合成能を明らかにするため、放射性同位体（RI）で標識された脂肪酸を用いて代謝実験を行った。本実験では、脂肪酸代謝酵素が高発現する脳や肝臓の分散細胞を調製したのち、RI 標識された ALA またはドコサペンタエン酸（DPA; 22:5n-3）の存在下で培養し、各細胞における代謝産物を追跡した。その結果、海産種 *G. melas* ではすべての区において DHA は検出されず、本種は多くの海産魚と同様に DHA 合成能をもたないことが明らかになった。一方、その他 3 種では、いずれも ALA および DPA 添加区から DHA が検出された。また、テトラコサペンタエン酸（TPA; 24:5n-3）やテトラコサヘキサエン酸（THA; 24:6n-3）は降河回遊種 *T. maculatus* ではほとんど検出されなかったが、淡水産の 2 種、特に *A. finis* では強く検出される傾向があった。このことから、生活史の一部、あるいは全部を淡水に依存するこれらの種は、ALA からの DHA 合成能を獲得していること

が明らかになり、3 種の DHA 合成経路には何らかの差異があることが示唆された。

そこで、アキルス科 4 種の DHA 合成経路を詳細に明らかにするため、脳や肝臓の cDNA から不飽和化酵素遺伝子（*fads2*）や鎖長延長酵素遺伝子（*elovl5*）を単離したのち、酵母発現系による機能解析を行った。その結果、海産種 *G. melas* は不飽和化酵素の機能欠損により DHA を合成できないことが明らかになった。一方、降河回遊種 *T. maculatus* は Δ4 活性を獲得した不飽和化酵素により Δ4 経路を駆動可能であり、淡水種 *A. finis* は炭素数 24 の脂肪酸の代謝能強化により Sprecher 経路を駆動可能であった。また、淡水種 *H. mentalis* では遺伝子重複により生じた活性の異なる 2 種の不飽和化酵素が不飽和化反応を分担し、Δ4 経路と Sprecher 経路の両方を駆動可能であった。このことから、淡水進出種では脂肪酸代謝酵素の機能が非常に多様化していながら、いずれの酵素機能の組み合わせも DHA 生合成という共通の結果を導いていることが明らかになり、彼らの間で貧 DHA 環境への適応を可能にする DHA 合成能の獲得という収斂進化が生じていることが強く示唆された。

以上の研究から、アキルス科魚類では DHA の豊富な海に留まる祖先的な種は DHA 合成能をもたず、淡水への進出を果たした分化的な種は様々な形で DHA 合成能を獲得していることが明らかになり、海産魚が淡水環境に適応するためには、低張環境における浸透圧調節能に並び、貧 DHA という栄養学的障壁を克服するための DHA 合成能の獲得が極めて重要な要素になるものと結論付けた。

Abstract

The colonisation of freshwater environments by marine fishes has historically been considered a result of adaptation to low osmolality. However, most marine fishes cannot synthesise the physiologically indispensable fatty acid, docosahexaenoic acid (DHA), due to incomplete DHA biosynthetic pathways, which must be adapted to survive in freshwater environments where DHA is poor relative to marine environments. By analysing DHA biosynthetic pathways of one marine and three freshwater-dependent species from the flatfish family Achiridae, we revealed that functions of fatty-acid metabolising enzymes have uniquely and independently evolved by multi-functionalisation or neofunctionalisation in each freshwater species, such that every functional combination of the enzymes has converged to generate complete and functional DHA biosynthetic pathways. Our results demonstrate the elaborate patchwork of fatty-acid metabolism and the importance of acquiring DHA biosynthetic function in order for fish to cross the nutritional barrier at the mouth of rivers and colonise freshwater environments.

Introduction

Docosahexaenoic acid (DHA; 22:6n–3), an omega-3 long-chain polyunsaturated fatty acid (LC-PUFA), is a crucial fatty acid that supports various functions of the cell membrane as a component of the lipid bilayer, owing to its structural flexibility, and further modulating physiological processes directly or as a precursor of bioactive derivatives[1,2,3,4]. It is obtained either as preformed DHA or can be synthesised in most vertebrates from α-linolenic acid (ALA; 18:3n–3; Fig. 1), which is a dietary essential fatty acid[4]. The first step in the DHA biosynthetic pathway is Δ6 desaturation of dietary ALA to 18:4n–3, followed by elongation to 20:4n–3 or, alternatively, elongation of ALA to 20:3n–3, followed by Δ8 desaturation to 20:4n–3. Then, using 20:4n–3 as a substrate, eicosapentaenoic acid (EPA; 20:5n–3) is produced by Δ5 desaturation. In teleost fishes that possess the ability to synthesise DHA, the production of DHA from EPA is achieved by two alternative routes, called the "Sprecher pathway" and "Δ4 pathway"[5,6,7]. The former consists of two consecutive elongations to produce 24:5n–3, followed by Δ6 desaturation to 24:6n–3 and chain shortening to DHA by β-oxidation at the end (Fig. 1). The latter route

is initiated by a single elongation to 22:5n–3, followed by the direct conversion to DHA via Δ4 desaturation. The desaturation and elongation reactions described above are catalysed by fatty acid desaturases (Fads) and elongation of very long-chain fatty acids (Elovl) proteins, respectively. These enzymes have their own substrate specificities to share the pathway and complete DHA biosynthesis by their concerted actions[5,7].

Spiny-rayed fishes (superorder Acanthopterygii), the largest and most diverse group of fishes, have a limited repertoire of enzymes for DHA biosynthesis[7,8,9]. In particular, marine Acanthopterygii possess only two enzymes, namely Fads2, which has Δ6/Δ8 desaturase activity[5,10], and Elovl5, which shows preferential elongase activity towards C_{18} and C_{20} substrates[11]. Moreover, it was previously demonstrated by functional characterisation in a heterologous expression system that Fads2 of marine Acanthopterygii have little or no Δ6 desaturase activity towards 24:5n–3[6]. Therefore, marine Acanthopterygii species strictly require DHA from their diet and develop fatal disorders if they are raised under DHA-deficient conditions[12,13]. A potential cause for the loss of DHA biosynthesis capability is low selective pressure due to the marine food web already being rich in DHA produced by marine microalgae and microbes[12,14]. Hence, marine

Acanthopterygii can easily satisfy their DHA requirements by feeding on their natural prey, despite their incomplete DHA biosynthetic pathway[15]. In contrast, the availability of DHA in freshwater prey is limited[15], as primary producers in the freshwater food web are characterised by containing substantial levels of ALA, but are generally poor in DHA[16]. The fact that freshwater species belonging to Osteoglossomorpha and Otophysi (the oldest living and most diverse freshwater teleost lineages, respectively[17,18]) possess the capability for DHA biosynthesis[8,19-22] suggests that dietary DHA obtained in the freshwater environment is not sufficient for normal development and survival. Still, some lineages of marine Acanthopterygii, which originally and exclusively relied on exogenous DHA, have successfully invaded and colonised freshwater environments[23,24]. Although the marine-to-freshwater transition has hitherto been attributed to substantial adaptation of the osmoregulatory system to overcome the osmotic barrier[25,26], there is another potential barrier that had to be conquered by Acanthopterygii species moving into the freshwater environment: the gap between the physiological demand and the dietary supply of DHA.

This study focused on flatfishes (Pleuronectiformes: Acanthopterygii) distributed in marine and freshwater environments to examine the nutritional barrier created by

DHA-deficient prey in fresh water and the adaptive mechanisms that may allow marine-origin Acanthopterygii to occupy freshwater habitats. Although this taxonomic order principally consists of marine species, many species from several families migrate to estuaries, which function as nursery grounds, and some even move up into rivers[27,28]. To understand the life histories and optimise the culture conditions of these ecologically and commercially important fishes, their salinity tolerance has been investigated intensively, and many families are categorised as euryhaline[29]. However, there have been no reports of any flatfish species with a complete DHA biosynthetic pathway from ALA[5,30]. Dietary DHA deficiency causes poor growth and survival and developmental abnormalities in marine flatfishes[31] and hence should result in decreased fitness under natural conditions. Indeed, only 10 out of the 772 species (1.3% of the total diversity) in this order are thought to be freshwater residents[28]. We consequently hypothesised that this nutritional barrier provides evolutionary pressure that obstructs flatfishes with low-salinity tolerance from attempting to colonise freshwater environments.

A family of Pleuronectiformes, Achiridae, commonly called American sole, which has expanded its habitat from the sea to rivers[32], is now distributed across the coastal area

of the Americas to the western Amazon. It comprises six genera containing approximately 35 species, from which six are restricted entirely to fresh water[28,33], and the different genera show varying tendencies in terms of habitat preference[33]. Hence, Achiridae is an interesting example of marine-derived Acanthopterygii that can be used to explore the physiological basis for habitat adaptation.

In this study, four Achiridae species were analysed: *Gymnachirus melas* (marine; distributed along the east coast of the USA, eastern Gulf of Mexico, and Bahamas[34]), *Trinectes maculatus* (catadromous; distributed along the eastern coast of North America from Maine (USA) to Mexico[35,36]), *Apionichthys finis* (freshwater; distributed through the Essequibo and middle and upper Amazon basins[37]), and *Hypoclinemus mentalis* (freshwater; distributed through the Amazon, Orinoco, and Essequibo basins[38]). First, we examined their migratory histories and phylogenetic relationships to illustrate freshwater colonisation of Achiridae. Second, the capabilities for DHA biosynthesis in the four species were investigated using brain and hepatic cells isolated from each species, cultured with radiolabelled fatty-acid substrates. Third, we conducted functional characterisation of fatty-acid metabolising enzymes and revealed their divergent functions, including, to our

knowledge, the first discovery of a trifunctional Δ4Δ5Δ6 Fads2, giving rise to different, yet fully functional and complete DHA biosynthetic pathways among the three freshwater species.

Results and discussion

Estimating migratory histories and phylogenetic relationships

We used otolith analysis to examine their environmental life histories, and specifically, to determine whether the so-called freshwater species had any previous exposure to marine conditions. Otoliths are biominerals present in the inner ears that are responsible for the sense of balance in teleost fishes. They consist predominantly of calcium carbonate and, for some short-lived teleosts, grow in proportion to somatic growth of the individual. Otoliths incorporate trace elements that reflect ambient environmental conditions, such as salinity[39]. We analysed the strontium (Sr) concentration, which is positively correlated to the ambient salinity, in transverse sections of the sagittal otoliths (Fig. 2a-c). In the marine species *G. melas*, the Sr concentration was high in the core and peripheral areas, indicating birth and residence predominantly in sea water (Fig. 2a). However, these otoliths also showed concentric regions with intermediate to low Sr concentration presumed to reflect transient forays into areas of low to moderate salinity, such as an estuary, often used as nursery grounds in this order[27]. The otoliths of *A. finis* and *H. mentalis* showed a low Sr concentration throughout the otolith (Fig. 2b, c), indicating that these fishes were born in

and never left the Amazon, where they were captured. Our results are in agreement with previous reports based on capture sites[33] and demonstrate that *A. finis* and *H. mentalis* spend their entire life in fresh water.

Next, we constructed a molecular phylogenetic tree with the closely related ancestral marine family Citharidae[40] as an outgroup using 16S rRNA genes (Fig. 3) to investigate the evolutionary relationships among the four species of Achiridae. The resultant tree, which is consistent with previous reports[41,42], showed *G. melas* as the first species branching from the lineage leading to *A. finis* and *H. mentalis* via the intermediate *T. maculatus*. Our phylogenetic tree suggests that *G. melas*, which relies heavily on marine habitats, maintains some ancestral physiological features associated with freshwater adaptation.

The low osmolality of the freshwater environment is an initial cause of disruption of homeostasis in marine fishes. To gain insight into when the lineage of Achiridae acquired the capability to cope with hypoosmotic stress, we compared the hypoosmotic tolerance of *G. melas* (Fig. 4) to that of the euryhaline *T. maculatus*[35,36,43] and a stenohaline marine Acanthopterygii, the horse mackerel (*Trachurus japonicus*)[44]. The test was carried

out by the gradual replacement of sea water (SW) with fresh water (FW) in a laboratory tank according to a schedule designed so that *T. maculatus* would survive. In this test, *G. melas* showed remarkable tolerance to survive in 10% SW, whereas all horse mackerel used in the study did not. This suggests that a substantial tolerance to low salinity is shared among Achiridae regardless of their natural habitat.

Tracing fatty-acid metabolism in brain and hepatic cells

We then examined the capability of Achiridae to synthesise DHA from ALA to determine whether there are differences that reflect the nutritional environment of each natural habitat (Fig. 5-8). For each of the four sole species we cultured cells from brain and liver, where Fads and Elovl are highly expressed[7], with radiolabelled [1-^{14}C]ALA or [1-^{14}C]22:5n–3. After 40 h of culture, total lipid was extracted from the cells to prepare fatty acid methyl esters (FAMEs), which were then developed with thin-layer chromatography (TLC). Although incorporation of [1-^{14}C]ALA and [1-^{14}C]22:5n–3 into the cells was detected, no radioactive DHA (22:6n–3) was detected in *G. melas* brain or hepatic cells (Fig. 5). However, we clearly found radioactive DHA along with a series of intermediates in the

FAMEs derived from the hepatic cells of the other three soles, which spend a substantial portion of their life cycle in the FW environment (Fig. 6-8). It is noteworthy that radioactive 24:5n–3 and 24:6n–3, which are the intermediates in the Sprecher pathway (Fig. 1), were detected in both *A. finis* and *H. mentalis*, but especially strong in *A. finis* (Fig. 7, 8). Moreover, radioactive DHA synthesised in the brain cells was detected only in *H. mentalis* (Fig. 8). Our data demonstrate that the three FW-dependent species possess the capability to synthesise DHA from ALA, whereas the marine species, *G. melas*, likely does not. Furthermore, the DHA biosynthetic pathways of the three FW-dependent species appeared to differ, particularly in the availability and utilisation of the Sprecher pathway.

Functional characterisation of Fads2 and Elovl5 enzymes

To investigate the molecular basis causing the above differences in DHA biosynthetic potency, we conducted functional characterisation of the enzymes Fads2 and Elovl5 involved in DHA biosynthesis with a heterologous expression system in yeast (*Saccharomyces cerevisiae*) (Fig. 9-15 and Table 1a-c)[45]. The Fads2 isolated from *G. melas* showed Δ6 activity towards ALA ($\Delta6_{18:3n-3}$), low Δ5, and no Δ4 desaturase activities (Fig.

13). In addition, its Δ6 activity towards 24:5n–3 ($\Delta6_{24:5n-3}$) was the lowest among the four sole species (Fig. 14). The *G. melas* Elovl5 exhibited activity towards C_{18} to C_{22} substrates (Table 1a) and production of 22:5n–3 and 24:5n–3 from EPA (20:5n–3, Fig. 15). In the DHA biosynthesis assay using *G. melas* cells, we observed only EPA biosynthesis from ALA in the brain cells and 24:5n–3 biosynthesis from 22:5n–3 in both the brain and hepatic cells (Fig. 5). Therefore, taken altogether, we concluded that *G. melas* is incapable of DHA biosynthesis due to insufficient activity of Fads2 to desaturate 22:5n–3 or 24:5n–3 (Fig. 16, red arrows).

In contrast, the Fads2 isolated from *T. maculatus* showed desaturase activity for the Δ6, Δ5, and Δ4 pathways (Fig. 13, 14). This conspicuous trifunctionality has not been reported in any other front-end desaturase known to date[7,10,46]. The Elovl5 showed elongase activities towards C_{18} to C_{22} substrates (Table 1a), although the production of 24:5n–3 from EPA was relatively low (Fig. 15), which is consistent with the weak radioactivity of 24:5n–3 detected in the DHA biosynthesis assay (Fig. 6). We concluded that *T. maculatus* synthesises DHA from ALA via the Δ4 pathway with the trifunctionalised Fads2 as a key enzyme in this process (Fig. 16, green arrows).

The Fads2 isolated from *A. finis* showed $\Delta 6_{18:3n-3}$, Δ5, and low Δ4 activities (Fig. 13) and performed $\Delta 6_{24:5n-3}$ desaturation at the highest efficiency among the four species (Fig. 14). The Elovl5 showed relatively high production of 24:5n–3 from EPA (Fig. 15), in addition to the conversion of C_{18} and C_{20} substrates (Table 1a). The results clearly supported the detection of radioactive C_{24} fatty acids in the DHA biosynthesis assay (Fig. 7), and we therefore concluded that *A. finis* conducts DHA biosynthesis from ALA with the enzymes reinforced to drive the Sprecher pathway (Fig. 16, blue arrows), which is weak or absent in the marine Acanthopterygii.

In the case of *H. mentalis*, we isolated two *fads2* genes sharing 98% identity at the deduced amino acid level and considered that the gene differentiated into paralogues after speciation because they formed a single branch in the molecular phylogenetic tree of Achiridae Fads2 (Fig. 17). The two Fads2, namely Fads2a and Fads2b, showed distinct activities, catalysing $\Delta 6_{18:3n-3}$ and Δ4 desaturation, respectively, while also showing Δ5 and $\Delta 6_{24:5n-3}$ activity (Fig. 13, 14 and Table 1b, c). The Elovl5 performed elongations of C_{18} to C_{22} substrates (Table 1a) and production of 22:5n–3 and 24:5n–3 from EPA (Fig. 15). These activities did not conflict with the moderate radioactivities of the C_{24} fatty acids

compared to those of *A. finis* in the DHA biosynthesis assay (Fig. 8). We concluded that *H. mentalis* synthesises DHA from ALA via both the Δ4 and Sprecher pathways, with the duplicated Fads2 specialised by neofunctionalisation to share the desaturation steps (Fig. 16, navy).

Exploring the molecular basis of Fads2 diversification

To further investigate the origin of the paralogous Fads2 of *H. mentalis*, we conducted PCR with four primers designed to map their genomic loci (Fig. 18a, b). The results demonstrated that they were located tandemly and exhibited conserved exon-intron boundaries (Fig. 18c), suggesting that gene duplication through unequal crossing-over occurred in this lineage[47]. We then analysed the relationship between the remarkable identity and divergent functions of the duplicated Fads2. They showed eight substitutions along their 442 amino acids (Fig. 19), with two of them located in the motif related to substrate preference, as demonstrated in previous studies (Fig. 20)[6,48]. We substituted each of the eight amino acids of Fads2b with those of Fads2a by site-directed mutagenesis, and, indeed, the mutant Fads2b lost Δ4 activity by altering Y277, which is well conserved in the

other Δ4Fads2 found in teleost fishes. On the other hand, the mutant Fads2a with Y277 introduced showed no Δ4 activity, while that carrying both F277Y and Q280H in the motif acquired a preference for Δ4 desaturation (Fig. 21 and Table 1d). Our results suggest that a few point mutations arose and directed the gene towards neofunctionalisation. Although duplications and neofunctionalisation of *fads2* genes are known in several other Acanthopterygii that are herbivorous, diadromous, or FW species[5,7], our finding in *H. mentalis* provides insight into the evolution of adaptive enzymes generated in the recent past, standing out from the other species in regard to the identity of paralogues. However, the trifunctional Fads2 of *T. maculatus* strays from the rule of the motif because it showed F280 conserved in the corresponding motif in Δ6Fads2 (Fig. 20) despite its Δ4 desaturase activity (Fig. 13). It seems that the unique mutations in other regions are responsible for the exceptional function of the enzyme in this species, while the structural basis is still unknown.

Our data reveal that independently accumulated mutations invited divergent functions of Fads2, and every combination, with Elovl5 showing different substrate

preferences, converged to complement the DHA biosynthetic pathway in each FW-dependent species of the family Achiridae. In other words, the genetic basis of each of these sole species has been utilised for a common outcome, DHA biosynthesis from ALA, and toward this end, every possible means has been implemented during natural selection (Fig. 22). Previously, it was demonstrated that a quantitative increase in the number of copies of *fads2* in the genome contributed to FW colonisation of sticklebacks by overcoming the constraint of low levels of dietary DHA[49]. Our work in Achiridae species highlights the FW nutritional barrier in a different light by demonstrating the qualitative alteration of the fatty-acid metabolising enzymes, with or without increases in the copy number of these genes, resulting in a variety of functionally complete DHA biosynthetic pathways. We therefore conclude that acquiring the capability for DHA biosynthesis from ALA, in addition to osmoregulation under low salinity, was a precondition for marine Acanthopterygii leaving the cradle filled with DHA and colonising freshwater environments.

Methods

Fish

Gymnachirus melas (12 individuals, standard length (SL) 90.7 ± 2.0 mm, body weight (BW) 17.7 ± 1.1 g, Fig. 23) captured in the western Atlantic Ocean were purchased from Quality Marine (Los Angeles, CA). *Trachurus japonicus* (4 individuals, SL 126.3 ± 3.8 mm, BW 37.0 ± 4.9 g) were caught in Tateyama Bay, Chiba, Japan. These two species were maintained in recirculating tanks with artificial seawater (33‰, 837 ± 1.2 mOsmol kg^{-1}; TetraMarin Salt Pro, Spectrum Brands Japan, Kanagawa, Japan) at 24°C and fed with the polychaete worm *Perinereis aibuhitensis* until use. *Trinectes maculatus* (26 individuals, SL 32.8 ± 2.1 mm, BW 1.3 ± 0.3 g, Fig. 24) were purchased from Ishi-to-Izumi (Tokyo, Japan), and *Apionichthys finis* (13 individuals, SL 52.5 ± 3.9 mm, BW 2.0 ± 0.7 g, Fig 25) and *Hypoclinemus mentalis* (3 individuals, 129.7 ± 2.9 mm, BW 55.7 ± 6.6 g, Fig. 26) were purchased from Ishi-to-Izumi or Kamihata Fish Industry (Hyogo, Japan). These three species were maintained in recirculating tanks with fresh water at 26°C and fed with frozen blood worms (larvae of Chironomidae), live sludge worms (*Tubifex tubifex*), or medaka

(*Oryzias latipes*). Zebrafish (*Danio rerio*) were maintained as described in a previous study[50]. All experiments were performed in accordance with the guidelines for the care and use of laboratory animals of the Tokyo University of Marine Science and Technology.

Phylogenetic analysis based on the 16S rRNA gene

Genomic DNA was extracted from the caudal fins of the four sole species using the Gentra Puregene Tissue Kit (QIAGEN, Venlo, Netherlands). The partial fragments of the 16S rRNA gene were PCR amplified using primers designed based on the orthologues in Achiridae collected from the GenBank database to anneal to conserved regions (Table 2, 3) with PrimeSTAR Max DNA polymerase (Takara Bio, Shiga, Japan). All PCR conditions in this research are summarised in Table 4. The PCR products were purified with the FastGene Gel/PCR Extraction Kit (Nippon Genetics, Tokyo, Japan) and cloned into the pGEM T-Easy Vector (Promega, Madison, WI) after adding 3’ adenosine overhangs with TaKaRa Taq (Takara Bio). The cloned PCR fragments were extracted using the FastGene Plasmid Mini Kit (Nippon Genetics) and sequenced using the BigDye Terminator v3.1 Cycle Sequencing Kit and ABI PRISM 3100-Avant Genetic Analyzer (Thermo Fisher

Scientific, Waltham, MA). The resulting sequences were assembled using CLC Main Workbench ver 6.7.1 (QIAGEN; Fig. 27-30 and Table 2) and aligned with the genes from *Citharoides macrolepidotus* (AP014588) and *Lepidoblepharon ophthalmolepis* (KJ433560), which belong to Citharidae, an ancestral family of Pleuronectiformes, using MAFFT v7.222 with the L-INS-i method[51,52]. After trimming gaps automatically using trimAl[53], a phylogenetic tree was constructed from the alignment made up of 960 columns by the maximum likelihood method using PhyML ver 3.0 server[54] with Smart Model Selection resulting in GTR+G+I, and the number of bootstrap replicates was set to 1000. The resulting tree was visualised in FigTree ver 1.4.3, available at http://tree.bio.ed.ac.uk/software/figtree/.

Estimating migratory history using otoliths

The strontium profiles in sagittal otoliths were analysed by electron probe microanalysis (EPMA) to obtain information on the environmental (salinity) history of the fishes. Otoliths were extracted from each individual, cleaned, dried, and embedded in UV-cured resin (Tama-koubou, Kanagawa, Japan)[55]. Each otolith was then ground transversally from

the postrostrum side using a series of 120-4000 grid abrasive paper on a grinder/polisher (Doctor-Lap ML-182; Maruto Instruments, Tokyo, Japan) to obtain a transversal section showing all preformed layers including the core region formed at birth. After course grinding, otoliths were further polished to a mirror-finish with 1 μm diamond paste on a polisher (Labopol-4; Struers, Ballerup, Denmark), cleaned and rinsed with deionised water prior, and dried. For EPMA, specimens were platinum/palladium-coated with an ion-sputter (E-1030; Hitachi High-Technologies Corporation, Tokyo, Japan) and analysed with an electron probe microanalyser (JXA-8230; JEOL, Tokyo, Japan) using strontium titanate (SrTiO3) as a reference standard. Maps of strontium concentration were generated with a focused beam set to 15 kV of accelerating voltage and 500 nA of beam current, with a pixel size of 2 μm and a dwell time of 40 ms.

Molecular cloning of *fads2*, *elovl5*, and *elovl2* genes

Total RNA was isolated from the brains and livers using ISOGEN reagent (Nippon Gene, Tokyo, Japan). After trace genomic DNA was eliminated with RQ1 RNase-Free DNase (Promega), the first-strand complementary DNA (cDNA) was synthesised using

Ready-To-Go You-Prime First-Strand Beads (GE Healthcare, Chicago, IL) with the oligo (dT) primer (Table 3) following the manufacturer's recommendations. The first fragment amplifications of *fads2*- and *elovl5*-like cDNA from *H. mentalis* and *T. maculatus* were carried out using the degenerate primers shown in Table 3, which were designed based on highly conserved regions of *fads2* and *elovl5* orthologues from several species of Pleuronectiformes (Table 2, 3) with TaKaRa Ex Taq polymerase (Takara Bio). To amplify the 5' and 3' ends of the cDNA, the rapid amplification of the cDNA ends (RACE) of both *fads2* and *elovl5*-like cDNA from the two species was performed using the GeneRacer Kit (Thermo Fisher Scientific) and the DNA polymerases, PrimeSTAR HS DNA polymerase and Tks Gflex DNA polymerase (Takara Bio). The gene-specific primers for 5' and 3'RACE are shown in Table 3. The purification, subcloning and sequencing of each PCR product was performed as described above without an A-tailing reaction. The resultant sequences were assembled to produce the full open reading frame (ORF) and amino acid sequeces were deduced using CLC Main Workbench ver 6.7.1 (QIAGEN; Fig. 31-40). The cDNA, including full ORFs, was PCR amplified using gene-specific primers that were annealed to the 5' and 3' untranslated regions (UTR) with PrimeSTAR Max DNA

polymerase. The *fads2*- and *elovl5*-like cDNAs from *G. melas* and *A. finis* were isolated using primers designed to anneal to the conserved regions in the 5' or 3' UTR of the two genes from the above two species (Table 3). The alignment of the deduced amino acid sequences of *fads2*- and *elovl5*-like cDNA, with several orthologues from the GenBank database, was conducted by MAFFT ver 7.222 with the L-INS-i method. After trimming gaps automatically using trimAl, a phylogenetic tree was constructed from the alignment made up of 445 columns by the maximum likelihood method using the PhyML ver 3.0 server with Smart Model Selection, resulting in LG+G+I, and the number of bootstrap replicates was set to 1000. The resulting tree was visualised in FigTree and rooted with Chondrichthyes Fads1 sequences.

Functional characterisation of Fads2 and Elovl5

The cDNAs corresponding to the *fads2* and *elovl5* ORFs of the four sole species and *fads2* and *elovl2* of zebrafish were PCR amplified using primers containing restriction enzyme sites of *Hin*dIII and *Xba*I for *fads2* and *elovl5* or *Hin*dIII and *Kpn*I for *elovl2* with PrimeSTAR Max DNA polymerase (Table 3). After gel purification following the method

described above, the PCR products were then digested by the corresponding restriction enzymes (*Hin*dIII, *Xba*I, and *Kpn*I; Takara Bio) and cloned into the yeast expression vector pYES2 (Thermo Fisher Scientific) digested by *Hin*dIII and *Xba*I for *fads2* and *elovl5* or pAUR123 (Takara Bio) digested by *Hin*dIII and *Kpn*I for *elovl2*. The mutations in *fads2a* and *fads2b* of *H. mentalis* in pYES2 were introduced by inverse PCR using the PrimeSTAR Mutagenesis Basal Kit (Takara Bio) and primers carrying each substitution shown in Table 3. Transformation with pYES2 vectors and the culture condition of INV*Sc*1 yeast (*Saccharomyces cerevisiae*; Thermo Fisher Scientific) were described in a previous study[45]. The following fatty acids (Larodan Fine Chemicals, Stockholm, Sweden) were used as substrates: 18:3n–3, 20:4n–3 and 22:5n–3 for the yeast transformed with *fads2* and 18:4n–3, 20:5n–3 and 22:5n–3 for *elovl5*. After 48 h of culture at 30°C in the presence of each substrate fatty acid, the yeast cells were collected, washed twice with ice-cold HBSS and lyophilised using a freeze dryer (FDU-1200; Tokyo Rikakikai, Tokyo, Japan). FAMEs were prepared from the pellets of yeast and analysed using a gas chromatograph (GC-2025; Shimadzu, Kyoto, Japan) equipped with a flame ionisation detector and a silica capillary column (L × I.D. 30 m × 0.32 mm, d_f 0.25 μm; SUPELCOWAX 10; Merck,

Darmstadt, Germany) as previously described[56]. Enzymatic activities were calculated as the proportion of fatty acid substrate converted to desaturated or elongated products with the following formula: [product area / (product area + substrate area)] × 100 (%).

To analyse the Δ6 activity towards 24:5n–3, we constructed co-expression vectors of Achiridae Fads2 and zebrafish Elovl2 using an In-Fusion HD Cloning Kit (Takara Bio). Isolation of the *elovl2* with PADH1 and TADH1 regions from the above pAUR123 vector as an insert and linearisation of the pYES2 vectors carrying each *fads2* were carried out by the primers designed as described in the manual and PrimeSTAR Max DNA polymerase. The recombinant yeast transformed by the resultant vectors were selected and cultured with 22:5n–3 as described above for 24 h, but without induction of the *fads2* connected to PGAL1 by galactose, to allow the elongation of 22:5n–3 to 24:5n–3 by the *elovl2* connected to PADH1, which is constitutively expressed. Then, 2% galactose was added to the yeast cultures for the induction of *fads2* to allow the desaturation of 24:5n–3 to 24:6n–3, and the cultures were further incubated for 48 h until collection. To standardise and compare the Δ6 activity towards 24:5n–3 in Achiridae Fads2, the yeast were cultured in the presence of 18:3n–3 as control according to the above process. The Δ6 activity

towards 24:5n–3 was calculated as described above, considering the areas of 24:5n–3 produced by Elovl2 as the substrate, then divided by the Δ6 activity in the control cultures for standardisation.

Analysis of the genomic loci of *Hmfads2a* and *Hmfads2b*

Two primer pairs were designed that anneal as described in Fig. 18a, but do not extend across the putative exon-intron junctions predicted from the genomic *fads2* structure of *Cynoglossus semilaevis* (Gene ID: 103380276). Genomic DNA fragments were amplified by PCR using combinations of primers (Table 3) with TaKaRa LA Taq and PrimeSTAR GXL DNA polymerase (Takara Bio). The products of TaKaRa LA Taq were used to determine the draft sequences. The resultant sequences were combined and annotated according to the CDS and untranslated regions based on the cDNA sequences and those of *C. semilaevis*.

Tracing fatty acid metabolism in cell culture

The capacity for endogenous PUFA biosynthesis in each species was examined using

radiolabelled fatty acid substrates. Brain and hepatic cells were collected from *G. melas*, *T. maculatus*, *A. finis*, and *H. mentalis*. The fishes were anaesthetised with 0.02% (v/v) 2-phenoxyethanol, and their bulbus arteriosus was incised to remove the blood with 10 U/ml heparin sodium in Hanks' balanced salt solution (HBSS) to prevent the contamination of red blood cells following culture. The isolated livers were minced and incubated with 2 mg/ml collagenase IV (C5138; Sigma-Aldrich, St. louis, MO) and 150 U/ml DNase I (D5025; Sigma-Aldrich) in HBSS for 4 h at 20°C. After incubation, the resultant hepatic cell suspensions were filtered and rinsed as described in a previous study[57]. The isolated brains were minced and filtered as described in a previous study[58].

For the LC-PUFA biosynthesis assays, all cell pellets were resuspended in L-15 medium (ThermoFisher Scientific) containing 50 µg/ml ampicillin sodium (FUJIFILM Wako Pure Chemical Corporation, Tokyo, Japan), 50 µg/ml streptomycin sulfate (FUJIFILM Wako) and 50 U/ml benzylpenicillin potassium (FUJIFILM Wako). For brain cultures, fetal bovine serum (ThermoFisher Scientific) was added to the medium at a 10% concentration. The 2 ml cell suspensions were dispensed into 6-well plates (*T. maculatus*: 1.2×10^7 hepatic and 7.0×10^6 brain cells, *A. finis*: 1.2×10^7 and 6.2×10^5 cells), or 5 ml

was dispensed into 25 cm^2 tissue culture flasks (*G. melas*: 2.1×10^7 and 1.8×10^7 cells, *H. mentalis*: 2.1×10^7 and 1.8×10^7 cells). The radiolabelled [1-^{14}C] 18:3n–3 or [1-^{14}C] 22:5n–3 (American Radiolabeled Chemicals, St. louis, MO) was conjugated with bovine serum albumin (BSA, fatty acid free, A8806; Sigma-Aldrich) as described in a previous study[57]. The cells were cultured with 3.7 kBq (2 nmol)/ml of the PUFA/BSA complexes at 20°C for 40 h. The cells were then harvested and centrifuged at 400 × g for 2 min to discard the supernatant and rinsed with 5 ml of HBSS containing 1% BSA. Total lipids were extracted from the cell pellets using chloroform/methanol (2:1, v/v) as described in previous studies[59,60]. Fatty acid methyl esters (FAMEs) were prepared from evaporated total lipids using a Fatty Acid Methylation Kit (Nacalai Tesque, Kyoto, Japan) and purified using a Fatty Acid Methyl Ester Purification Kit (Nacalai Tesque) following the manufacturer's instructions. FAMEs were concentrated in 1 ml of hexane, and 400 µl was applied as 1 cm streaks to thin layer chromatography (TLC, 20 cm × 20 cm; Merck) plates, which were pre-immersed in 0.1 mg/ml silver nitrate in acetonitrile for 10 min and activated at 110°C for 30 min. The plates were developed in toluene/acetonitrile (95:5, v/v) and subjected to autoradiography using imaging plates with an image analyser (FLA-9000;

Fujifilm, Tokyo, Japan).

The radiolabelled [1-^{14}C] fatty acids for the standard mixture were purchased from American Radiolabeled Chemicals (18:3n–3, 20:3n–3, 20:5n–3, and 22:5n–3) or Moravek (22:5n–3 and 22:6n–3; Brea, CA). These were mixed to 370 Bq each and methyl-esterified as described above to create 1 ml of standard solution (except 20:4n–3) in hexane. The other standards for intermediate metabolites in the DHA biosynthetic pathway, 20:4n–3 and 24:6n–3, were biosynthesised from 18:4n–3 and 24:5n–3 (American Radiolabeled Chemicals) by the yeast transformed with pYES2 carrying *elovl5* from *Nibea mitsukurii*[56] and *fads2* from *D. rerio*, respectively, following the above method. The yeast were cultured with 3.7 kBq of the fatty acids and lysed by incubation with 50 µl of 30 mg/ml zymolyase (Nacalai Tesque) at 37°C for 30 min. The total lipids of these lysates were extracted, methylated, and purified as described above to create 1 ml of metabolite solutions in hexane. The final standard mixture was prepared by mixing 100 µl each of the standard solutions (except 20:4n–3) and the metabolite solution of 18:4n–3. The positions where 24:5n–3 and 24:6n–3 appeared on the TLC plates were confirmed using the metabolite solution of 24:5n–3 (Fig. 41).

Acclimation test for hypoosmolality

To examine survival of *G. melas*, *Trinectes maculatus*, and *Trachurus japonicus* in hypoosomotic condition, individuals of these species were exposed to hypoosmolality by discarding half a tank of water and refilling the tank gradually with fresh water or diluted seawater (SW) using siphon effect for around 12 h according to the following schedule over 12 days: 50%, 40%, 30%, 20%, and 10% SW for 2 days each. After acclimation to 10% SW, the tank water was further diluted to 5% and 2.5% for 1 day each.

Statistics and Reproducibility

The otolith data were obtained from six, four, and six individuals of *Gymnachirus melas*, *Apionichthys finis*, and *Hypoclinemus mentalis*, respectively, and representative data were shown. Bootstrap values are shown next to each branch point of the phylogenetic trees. The Fads2 and Elovl5 enzymes were functionally characterised using the coding sequence of each encoding gene isolated from one representative individual of each species. The PCR amplifications of genomic *fads2* were performed with template DNA purified from

three individuals of *H. mentalis* and all of them showed identical amplification patterns.

Data Availability

All datasets generated during and/or analysed during the current study are available from the corresponding author by reasonable request. The accession numbers of all sequence data determined in this study are listed in Table 2.

References

1. Spector, A. A. Essentiality of fatty acids. *Lipids* **34**, S1–S3 (1999).

2. Tocher, D. R. Metabolism and functions of lipids and fatty acids in teleost fish. *Rev. Fish. Sci.* **11**, 107–184 (2003).

3. Wassall, S. R. & Stillwell, W. Docosahexaenoic acid domains: the ultimate non-raft membrane domain. *Chem. Phys. Lipids* **153**, 57–63 (2008).

4. Horrocks, L. A. & Farooqui, A. A. Docosahexaenoic acid in the diet: its importance in maintenance and restoration of neural membrane function. *Prostaglandins Leukot. Essent. Fat. Acids* **70**, 361–372 (2004).

5. Castro, L. F. C., Tocher, D. R. & Monroig, Ó. Long-chain polyunsaturated fatty acid biosynthesis in chordates: insights into the evolution of Fads and Elovl gene repertoire. *Prog. Lipid Res.* **62**, 25–40 (2016).

6. Oboh, A. *et al.* Two alternative pathways for docosahexaenoic acid (DHA, 22:6n-3) biosynthesis are widespread among teleost fish. *Sci. Rep.* **7**, 1–10 (2017).

7. Monroig, Ó., Tocher, D. R. & Castro, L. F. C. Polyunsaturated fatty acid

biosynthesis and metabolism in fish. in *Polyunsaturated Fatty Acid Metabolism* (ed. Burdge, G. C.) 31–60 (Elsevier, 2018).

8. Lopes-Marques, M. *et al.* Retention of fatty acyl desaturase 1 (*fads1*) in Elopomorpha and Cyclostomata provides novel insights into the evolution of long-chain polyunsaturated fatty acid biosynthesis in vertebrates. *BMC Evol. Biol.* **18**, 1–9 (2018).

9. Machado, A. M. *et al.* "Out of the can": a draft genome assembly, liver transcriptome, and nutrigenomics of the european sardine, *sardina pilchardus*. *Genes (Basel).* **9**, 1–13 (2018).

10. Kabeya, N., Yoshizaki, G., Tocher, D. R. & Monroig, Ó. Diversification of Fads2 in finfish species: implications for aquaculture. in *Investigación y desarrollo en nutrición acuícola* (eds. Cruz-Suárez, L. E. *et al*.) 338–362 (Universidad Autónoma de Nuevo León, 2017).

11. Monroig, Ó. *et al.* Evolutionary functional elaboration of the *Elovl2/5* gene family in chordates. *Sci. Rep.* **6**, 1–10 (2016).

12. Tocher, D. R. Fatty acid requirements in ontogeny of marine and freshwater fish.

Aquac. Res. **41**, 717–732 (2010).

13. Mesa-Rodriguez, A. *et al*. Effect of increasing docosahexaenoic acid content in weaning diets on survival, growth and skeletal anomalies of longfin yellowtail (*Seriola rivoliana*, Valenciennes 1833). *Aquac. Res.* **49**, 1200–1209 (2018).

14. Gladyshev, M. I., Sushchik, N. N. & Makhutova, O. N. Production of EPA and DHA in aquatic ecosystems and their transfer to the land. *Prostaglandins Other Lipid Mediat.* **107**, 117–126 (2013).

15. Bell, M. V. & Tocher, D. R. Biosynthesis of polyunsaturated fatty acids in aquatic ecosystems: general pathways and new directions. in *Lipids in Aquatic Ecosystems* (eds. Arts, T. M., Brett, M. T. & Kainz, J. M.) 211–236 (Springer, 2009).

16. Twining, C. W., Brenna, J. T., Hairston, N. G. & Flecker, A. S. Highly unsaturated fatty acids in nature: what we know and what we need to learn. *Oikos* **125**, 749–760 (2016).

17. Hilton, E. J. & Lavoué, S. A review of the systematic biology of fossil and living bony-tongue fishes, Osteoglossomorpha (Actinopterygii: Teleostei). *Neotrop. Ichthyol.* **16**, e180031 (2018).

18. Chen, W. J., Lavoué, S. & Mayden, R. L. Evolutionary origin and early biogeography of Otophysian fishes (Ostariophysi: Telostei). *Evolution* **67**, 2218–2239 (2013).

19. Monroig, Ó., Rotllant, J., Sánchez, E., Cerdá-Reverter, J. M. & Tocher, D. R. Expression of long-chain polyunsaturated fatty acid (LC-PUFA) biosynthesis genes during zebrafish *Danio rerio* early embryogenesis. *Biochim. Biophys. Acta - Mol. Cell Biol. Lipids* **1791**, 1093–1101 (2009).

20. Oboh, A., Betancor, M. B., Tocher, D. R. & Monroig, Ó. Biosynthesis of long-chain polyunsaturated fatty acids in the African catfish *Clarias gariepinus*: molecular cloning and functional characterisation of fatty acyl desaturase (*fads2*) and elongase (*elovl2*) cDNAs. *Aquaculture* **462**, 70–79 (2016).

21. Janaranjani, M. *et al.* Capacity for eicosapentaenoic acid and arachidonic acid biosynthesis in silver barb (*Barbonymus gonionotus*): functional characterisation of a Δ6/Δ8/Δ5 Fads2 desaturase and Elovl5 elongase. *Aquaculture* **497**, 469–486 (2018).

22. Ferraz, R. B. *et al.* A complete enzymatic capacity for long-chain polyunsaturated

fatty acid biosynthesis is present in the Amazonian teleost tambaqui, *Colossoma macropomum*. *Comp. Biochem. Physiol. Part - B Biochem. Mol. Biol.* **227**, 90–97 (2019).

23. Berra, T. M. *Freshwater Fish Distribution*. (University of Chicago Press, 2007).

24. Carrete Vega, G. & Wiens, J. J. Why are there so few fish in the sea? *Proc. R. Soc. B Biol. Sci.* **279**, 2323–2329 (2012).

25. Lee, C. E. & Bell, M. A. Causes and consequences of recent freshwater invasions by saltwater animals. *Trends Ecol. Evol.* **14**, 284–288 (1999).

26. Yamanoue, Y. *et al.* Multiple invasions into freshwater by pufferfishes (Teleostei: Tetraodontidae): A mitogenomic perspective. *PLoS One* **6**, (2011).

27. Able, K. W. & Fodrie, F. J. Distribution and dynamics of habitat use by juvenile and adult flatfishes. in *Flatfish: Biology and Exploitation, Second Edition* (eds. Gibson, R. N., Nash, R. D. M., Geffen, A. J. & van der Veer, H. W.) 242–282 (John Wiley & Sons, Ltd, 2014).

28. Nelson, J. S., Grande, T. C. & Wilson, M. V. H. *Fishes of the World, Fifth Edition*. (John Wiley & Sons, Inc, 2016).

29. Ruiz-Jarabo, I. *et al.* Environmental salinity and osmoregulatory processes in cultured flatfish. *Aquac. Res.* **46**, 10–29 (2015).

30. Kabeya, N., Chiba, M., Haga, Y., Satoh, S. & Yoshizaki, G. Cloning and functional characterization of *fads2* desaturase and *elovl5* elongase from Japanese flounder *Paralichthys olivaceus*. *Comp. Biochem. Physiol. Part - B Biochem. Mol. Biol.* **214**, 36–46 (2017).

31. Bell, J. G., McEvoy, L. A., Estevez, A., Shields, R. J. & Sargent, J. R. Optimising lipid nutrition in first-feeding flatfish larvae. *Aquaculture* **227**, 211–220 (2003).

32. Munroe, T. A. Distributions and biogeography. in *Flatfish: Biology and Exploitation, Second Edition* (eds. Gibson, R. N., Nash, R. D. M., Geffen, A. J. & van der Veer, H. W.) 52–82 (John Wiley & Sons, Ltd, 2014).

33. Fricke, R., Eschmeyer, W. N. & Van der Laan, R. *Eschmeyer's Catalog of Fishes: Genera, Species, References.* http://researcharchive.calacademy.org/research/ichthyology/catalog/fishcatmain.asp (2019).

34. Dawson, C. E. A revision of the western Atlantic flatfish genus *Gymnachirus* (the

naked soles). *Copeia* **4**, 646–665 (1964).

35. Dovel, W. L., Mihursky, J. A. & McErlean, A. J. Life history aspects of the hogchoker, *Trinectes maculatus*, in the Patuxent River Estuary, Maryland. *Chesap. Sci.* **10**, 104–119 (1969).

36. Peterson, T. L. Seasonal migration in the southern hogchoker, *Trinectes maculatus fasciatus* (Achiridae). *Gulf Res. Rep.* **9**, 169–176 (1996).

37. Ramos R. T. C. Systematic review of *Apionichthys* (Pleuronectiformes: Achiridae), with description of four new species. *Ichthyol. Explor. Freshwaters* **14**, 97–126 (2003).

38. Reis, R. R., Kullander, S. O., Ferraris, C. J. *Checklist of the Freshwater Fishes of South and Central America*. (Edipucrs, 1996).

39. Campana, S. E. Chemistry and composition of fish otoliths: pathways, mechanisms and applications. *Mar. Ecol. Prog. Ser.* **188**, 263–297 (1999).

40. Betancur, R. R. *et al.* Phylogenetic classification of bony fishes. *BMC Evol. Biol.* **17**, 1–40 (2017).

41. Betancur, R., Li, C., Munroe, T. A., Ballesteros, J. A. & Ortí, G. Addressing gene

tree discordance and non-stationarity to resolve a multi-locus phylogeny of the flatfishes (Teleostei: Pleuronectiformes). *Syst. Biol.* **62**, 763–785 (2013).

42. Betancur-R, R. & Ortí, G. Molecular evidence for the monophyly of flatfishes (Carangimorpharia: Pleuronectiformes). *Mol. Phylogenet. Evol.* **73**, 18–22 (2014).

43. Peterson-Curtis, T. L. Effects of salinity on survival, growth, metabolism, and behavior in juvenile hogchokers, *Trinectes maculatus fasciatus* (Achiridae). *Environ. Biol. Fishes* **49**, 323–331 (1997).

44. Akamoto, T. S. Hormonal regulation of body fluid in teleost fishes. *Bull. Soc. Sea Water Sci. Japan* **69**, 244–246 (2015).

45. Li, Y. *et al.* Vertebrate fatty acyl desaturase with Δ4 activity. *Proc. Natl. Acad. Sci.* **107**, 16840–16845 (2010).

46. Monroig, Ó. & Kabeya, N. Desaturases and elongases involved in polyunsaturated fatty acid biosynthesis in aquatic invertebrates: a comprehensive review. *Fish. Sci.* **84**, 911–928 (2018).

47. Zhang, J. Evolution by gene duplication: an update. *Trends Ecol. Evol.* **18**, 292–298 (2003).

48. Lim, Z. L., Senger, T. & Vrinten, P. Four amino acid residues influence the substrate chain-length and regioselectivity of *Siganus canaliculatus* Δ4 and Δ5/6 desaturases. *Lipids* **49**, 357–367 (2014).

49. Ishikawa, A. *et al*. A key metabolic gene for recurrent freshwater colonizatioin and radiation in fishes. *Science* **364**, 886–889 (2019).

50. Li, Q., Fujii, W., Naito, K. & Yoshizaki, G. Application of *dead end*-knockout zebrafish as recipients of germ cell transplantation. *Mol. Reprod. Dev.* **84**, 1100–1111 (2017).

51. Katoh, K., Misawa, K., Kuma, K. & Miyata, T. MAFFT: a novel method for rapid multiple sequence alignment based on fast Fourier transform. *Nucleic Acids Res.* **30**, 3059–3066 (2002).

52. Katoh, K. & Standley, D. M. MAFFT multiple sequence alignment software version 7: improvements in performance and usability. *Mol. Biol. Evol.* **30**, 772–780 (2013).

53. Capella-Gutiérrez, S., Silla-Martínez, J. M. & Gabaldón, T. trimAl: a tool for automated alignment trimming in large-scale phylogenetic analyses. *Bioinformatics* **25**, 1972–1973 (2009).

54. Guindon, S. *et al.* New algorithms and methods to estimate maximum-likelihood phylogenies: assessing the performance of PhyML 3.0. *Syst. Biol.* **59**, 307–321 (2010).

55. Strüssmann, C. A., Miyoshi, K. & Mitsui, S. Application of UV-cured resin as embedding/mounting media for practical, time-saving otolith specimen preparation. *bioRxiv* 474643 (2018). doi:10.1101/474643

56. Kabeya, N. *et al.* Polyunsaturated fatty acid metabolism in a marine teleost, Nibe croaker *Nibea mitsukurii*: functional characterization of Fads2 desaturase and Elovl5 and Elovl4 elongases. *Comp. Biochem. Physiol. Part - B Biochem. Mol. Biol.* **188**, 37–45 (2015).

57. Bell, J. G. *et al.* The effect of dietary lipid on polyunsaturated fatty acid metabolism in Atlantic salmon (*Salmo salar*) undergoing parr-smolt transformation. *Lipids* **32**, 515–525 (1997).

58. Tocher, D. R. & Sargent, J. R. Incorporation into phospholipid classes and metabolism via desaturation and elongation of various 14C-labelled (n-3) and (n-6) polyunsaturated fatty acids in trout astrocytes in primary culture. *J. Neurochem.* **54**,

2118–2124 (1990).

59. Folch, J., Lees, M. & Sloane Stanley, G. H. A simple method for the isolation and purification of total lipides from animal tissues. *J. Biol. Chem.* **226**, 497–509 (1957).

60. Tocher, D. R., Sargen, J. R. & Frerichs, G. N. The fatty acid compositions of established fish cell lines after long-term culture in mammalian sera. *Fish Physiol. Biochem.* **5**, 219–227 (1988).

Figure Legends

Fig. 1

Fatty acids are represented by the n–x system of nomenclature. Desaturation and elongation steps are indicated by white arrows with the position of the double bond to be introduced and black arrows with carbon chain length, respectively. The two alternative pathways used to synthesise DHA from 22:5n–3 are coloured with orange and blue for the Sprecher pathway and Δ4 pathway, respectively.

Fig. 2

Representative maps of strontium (Sr) concentration in cross sections of otoliths from three Achiridae species including a marine species (**a**, *G. melas* [n = 6]) and two freshwater species (**b**, *A. finis* [n = 4] and **c**, *H. mentalis* [n = 6]). Scale bar = 500 µm.

Fig. 3

Phylogenetic tree of Achiridae and Citharidae (as an outgroup) based on the 16S rRNA

gene (partial sequence, 958 bp) shown along with their habitats.

Fig. 4

The dilution level of seawater (SW, %) and survival rate (%) of each species examined are represented by the blue line and the color of each bar, respectively. Gm: *Gymnachirus melas* (pink), Tm: *Trinectes maculatus* (green), Tj: *Trachurus japonicus* (purple).

Fig. 5

Autoradiography of TLC plate-developed radiolabelled fatty acid methyl esters (FAMEs) prepared from brain and hepatic cells of *Gymnachirus melas* cultured with radiolabelled α–linolenic acid (ALA, 18:3n–3) or 22:5n–3. 24:5n–3 and 24:6n–3 are indicated by asterisks and daggers, respectively. S, Standard mixtures of FAME.

Fig. 6

Autoradiography of TLC plate-developed radiolabelled FAMEs prepared from brain and hepatic cells of *Trinectes maculatus* cultured with radiolabelled 18:3n–3 or 22:5n–3.

24:5n–3 and 24:6n–3 are indicated by asterisks and daggers, respectively. S, Standard mixtures of FAME.

Fig. 7

Autoradiography of TLC plate-developed radiolabelled FAMEs prepared from brain and hepatic cells of *Apionichthys finis* cultured with radiolabelled 18:3n–3 or 22:5n–3. 24:5n–3 and 24:6n–3 are indicated by asterisks and daggers, respectively. S, Standard mixtures of FAME.

Fig. 8

Autoradiography of TLC plate-developed radiolabelled FAMEs prepared from brain and hepatic cells of *Hypoclinemus mentalis* cultured with radiolabelled 18:3n–3 or 22:5n–3. 24:5n–3 and 24:6n–3 are indicated by asterisks and daggers, respectively. S, Standard mixtures of FAME.

Fig. 9

Gas chromatograms of fatty acid methyl esters (FAMEs) isolated from recombinant yeast expressing *G. melas* Fads2 (**a-c**), *G. melas* Elovl5 (**d-f**), or *Danio rerio* Elovl2 and *G. melas* Fads2 (**g**, **h**). The yeast were grown with the exogenously added fatty acid substrate indicated by an asterisk: 18:3n–3 (**a**, **g**), 20:4n–3 (**b**), 22:5n–3 (**c**, **f**, **h**), 18:4n–3 (**d**), and 20:5n–3 (**e**). The inset in **h** shows a magnification of the time when 24:5n–3 and 24:6n–3 appeared.

Fig. 10

Gas chromatograms of fatty acid methyl esters (FAMEs) isolated from recombinant yeast expressing *T. maculatus* Fads2 (**a-c**), *T. maculatus* Elovl5 (**d-f**), or *D. rerio* Elovl2 and *T. maculatus* Fads2 (**g**, **h**). The yeast were grown with the exogenously added fatty acid substrate indicated by an asterisk: 18:3n–3 (**a**, **g**), 20:4n–3 (**b**), 22:5n–3 (**c**, **f**, **h**), 18:4n–3 (**d**), and 20:5n–3 (**e**). The inset in **h** shows a magnification of the time when 24:5n–3 and 24:6n–3 appeared.

Fig. 11

Gas chromatograms of fatty acid methyl esters (FAMEs) isolated from recombinant yeast expressing *A. finis* Fads2 (**a-c**), *A. finis* Elovl5 (**d-f**), or *D. rerio* Elovl2 and *A. finis* Fads2 (**g**, **h**). The yeast were grown with the exogenously added fatty acid substrate indicated by an asterisk: 18:3n–3 (**a**, **g**), 20:4n–3 (**b**), 22:5n–3 (**c**, **f**, **h**), 18:4n–3 (**d**), and 20:5n–3 (**e**). The inset in **h** shows a magnification of the time when 24:5n–3 and 24:6n–3 appeared.

Fig. 12

Gas chromatograms of fatty acid methyl esters (FAMEs) isolated from recombinant yeast expressing *H. mentalis* Fads2a (**a-c**), *H. mentalis* Fads2b (**d-f**), *H. mentalis* Elovl5 (**g-i**), *D. rerio* Elovl2 and *H. mentalis* Fads2a (**j**, **k**), or *D. rerio* Elovl2 and *H. mentalis* Fads2b (**l**, **m**). The yeast were grown with the exogenously added fatty acid substrate indicated by an asterisk: 18:3n–3 (**a**, **d**, **j**, **l**), 20:4n–3 (**b, e**), 22:5n–3 (**c**, **f**, **i**, **k**, **m**), 18:4n–3 (**g**), and 20:5n–3 (**h**). The insets in **k** and **m** show a magnification of the times when 24:5n–3 and 24:6n–3 appeared.

Fig. 13

The ratio among three desaturase activities of fatty acid desaturase 2 (Fads2) isolated from each Achiridae species when the total conversion rates are 100%, characterised by the yeast expression system. Relative conversion rates of Δ6 towards 18:3n–3 ($\Delta6_{18}$), Δ5 and Δ4 desaturation are shown as dark blue, blue and light blue bars, respectively. Gm: *Gymnachirus melas*, Tm: *Trinectes maculatus*, Af: *Apionichthys finis*, Hm: *Hypoclinemus mentalis*.

Fig. 14

Relative Δ6 activities towards 24:5n–3 of the Achiridae Fads2 normalised by those of 18:3n–3 when expressed with the zebrafish Elovl2 in yeast to produce 24:5n–3 from 22:5n–3.

Fig. 15

The ratio of eicosapentaenoic acid (EPA, 20:5n–3, dark orange), 22:5n–3 (orange) and 24:5n–3 (light orange) extracted from yeast cultured with EPA as the substrate and expressed elongation of very long chain fatty acid 5 (Elovl5) isolated from each Achiridae

species.

Fig. 16

The DHA biosynthetic pathway from 18:3n–3 with enzymatic activities of Fads2 and Elovl5 isolated from each Achiridae species estimated by the radiolabelled metabolites in the cell culture and fatty acid profiles of the yeast expressing recombinant enzymes. Each colour of arrow shows the activity of enzymes isolated from different species (red: *Gymnachirus melas*, green: *Trinectes maculatus*, blue: *Apionichthys finis*, navy: *Hypoclinemus mentalis*). Bold and narrow lines indicate high and low activities, respectively.

Fig. 17

Maximum likelihood phylogeny of Fads2 is shown. Achiridae Fads2 is highlighted with a blue background. The bootstrap values are shown at the nodes. The functionally characterised Fads2 were shown with their substrate specificities.

Fig. 18

a, Four primers (5'F, 5'R, 3'F and 3'R) were designed to anneal to conserved regions near both ends of the coding sequences (CDS) of the two *fads2* genes to analyse their genomic loci. **b,** Representative electrophoretic image of genomic PCR products from three individuals using the four primers independently or in pairs. Major bands were amplified by the four combinations of the primers (5F×5R, 5F×3R, 5R×3F, and 3F×3R). **c,** Genomic loci of the two *fads2* genes were predicted by the distribution of the primers and sequencing analysis of the PCR products derived from one representative individual. Regions of the genes, exons and CDS were annotated by blue, green and yellow arrows, respectively.

Fig. 19

Alignment of deduced amino acid sequences of two *H. mentalis* Fads2 proteins is shown. Identical residues are indicated with dots and shaded in black. The heme-binding motif (HPGG) and three histidine boxes (HXXXH, HXXHH, and QXXHH) are conserved in the

Fads family. The motif related to substrate specificity, or regioselectivity (Regio), is also indicated.

Fig. 20

The amino acid sequence alignment of the key residues (indicated by asterisks) for determining the regioselectivity of Fads2 isolated from Achiridae and several teleosts shown with their corresponding desaturase activity characterised in this study (Achiridae species) or reviewed previously (other species)[15]. Sc: *Siganus canaliculatus*, Ce: *Chirostoma estor*, Cs: *Channa striata*, On: *Oreochromis niloticus*, Po: *Paralichthys olivaceus*, Sm: *Scophthalmus maximus*, Ss: *Solea senegalensis*.

Fig. 21

The ratio of Δ4 activity to Δ6 activity towards 18:3n–3 of Fads2a, Fads2b and ten mutant Fads2 carrying substituted residue(s) that differed between the two Fads2 of *H. mentalis*.

Fig. 22

The marine species *G. melas* is unable to synthesise DHA due to the absence or inefficiency of Fads2 activities to desaturate at the Δ4 position or Δ6 position of 24:5n–3. The catadromous species *T. maculatus* has a multi-functionalised Fads2, which alone can catalyse Δ6, Δ5 and Δ4 desaturations to drive the Δ4 pathway. *A. finis* has reinforced Fads2 and Elovl5, which can catalyse C24 fatty acids more efficiently to drive the Sprecher pathway. *H. mentalis* possesses an additional highly homologous Fads2 (Fads2b) that performs Δ4 desaturation, which occurred via neofunctionalisation following gene duplication.

Fig. 23

The pictures of representative individuals of *Gymnachirus melas* are shown.

Fig. 24

The pictures of representative individuals of *Trinectes maculatus melas* are shown.

Fig. 25

The pictures of representative individuals of *Apionichthy finis* are shown.

Fig. 26

The pictures of represetative individuals of *Hypoclinemus mentalis* are shown.

Fig. 27

The partial sequence of 16S rRNA gene isolated from *Gymnachirus melas* is shown.

Fig. 28

The partial sequence of 16S rRNA gene isolated from *Trinectes maculatus* is shown.

Fig. 29

The partial sequence of 16S rRNA gene isolated from *Apionichthys finis* is shown.

Fig. 30

The partial sequence of 16S rRNA gene isolated from *Hypoclinemus mentalis* is shown.

Fig. 31

The partial sequence of *fads2* mRNA isolated from *Gymnachirus melas* annotated its coding sequence with yellow arrow and deduced amino acid sequence of its translated protein are shown.

Fig. 32

The complete sequence of *fads2* mRNA isolated from *Trinectes maculatus* annotated its coding sequence with yellow arrow and deduced amino acid sequence of its translated protein are shown.

Fig. 33

The partial sequence of *fads2* mRNA isolated from *Apionichthys finis* annotated its coding sequence with yellow arrow and deduced amino acid sequence of its translated protein are shown.

Fig. 34

The coding sequence of *fads2a* mRNA isolated from *Hypoclinemus mentalis* and deduced amino acid sequence of its translated protein are shown.

Fig. 35

The coding sequence of *fads2b* mRNA isolated from *Hypoclinemus mentalis* and deduced amino acid sequence of its translated protein are shown.

Fig. 36

The complete 5’ and 3’ untranslated region (UTR) sequence of *fads2a* and/or *fads2b* mRNA isolated from *Hypoclinemus mentalis* are shown. It was not precisely determined whether these UTR were shared by two transcripts because of their remarkable homology in coding sequences where primers used for RACE were designed.

Fig. 37

The partial sequence of *elovl5* mRNA isolated from *Gymnachirus melas* annotated its coding sequence with yellow arrow and deduced amino acid sequence of its translated

protein are shown.

Fig. 38

The complete sequence of *elovl5* mRNA isolated from *Trinectes maculatus* annotated its coding sequence with yellow arrow and deduced amino acid sequence of its translated protein are shown.

Fig. 39

The partial sequence of *elovl5* mRNA isolated from *Apionichthys finis* annotated its coding sequence with yellow arrow and deduced amino acid sequence of its translated protein are shown.

Fig. 40

The complete sequence of *elovl5* mRNA isolated from *Hypoclinemus mentalis* annotated its coding sequence with yellow arrow and deduced amino acid sequence of its translated protein are shown.

Fig. 41

Autoradiography of TLC plate-developed radiolabelled fatty acid methyl esters (FAMEs) is shown to indicate positions of 24:5n–3 and 24:6n–3. Standards for 20:4n–3 and 24:6n–3 were biosynthesised from 18:4n–3 and 24:5n–3 by the yeast transformed with pYES2 carrying *elovl5* from *Nibea mitsukurii* and *fads2* from *D. rerio*, respectively, and confirmed their positions by developing along with the other FAME standards.

Fig. 1

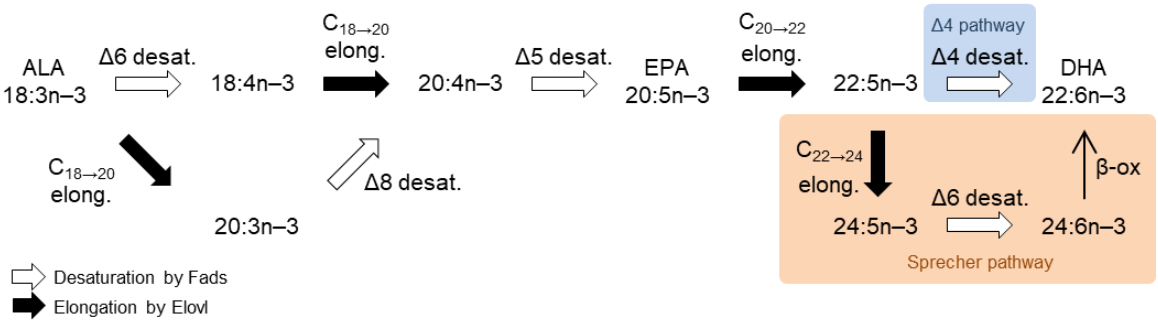
ALA
18:3n–3
Δ6 desat.
18:4n–3
C18→20
elong.
20:4n–3
Δ5 desat.
EPA
20:5n–3
C20→22
elong.
22:5n–3
Δ4 pathway
Δ4 desat.
DHA
22:6n–3
C18→20
elong.
20:3n–3
Δ8 desat.
C22→24
elong.
24:5n–3
Δ6 desat.
24:6n–3
β-ox
Sprecher pathway
Desaturation by Fads
Elongation by Elovl

Fig. 2

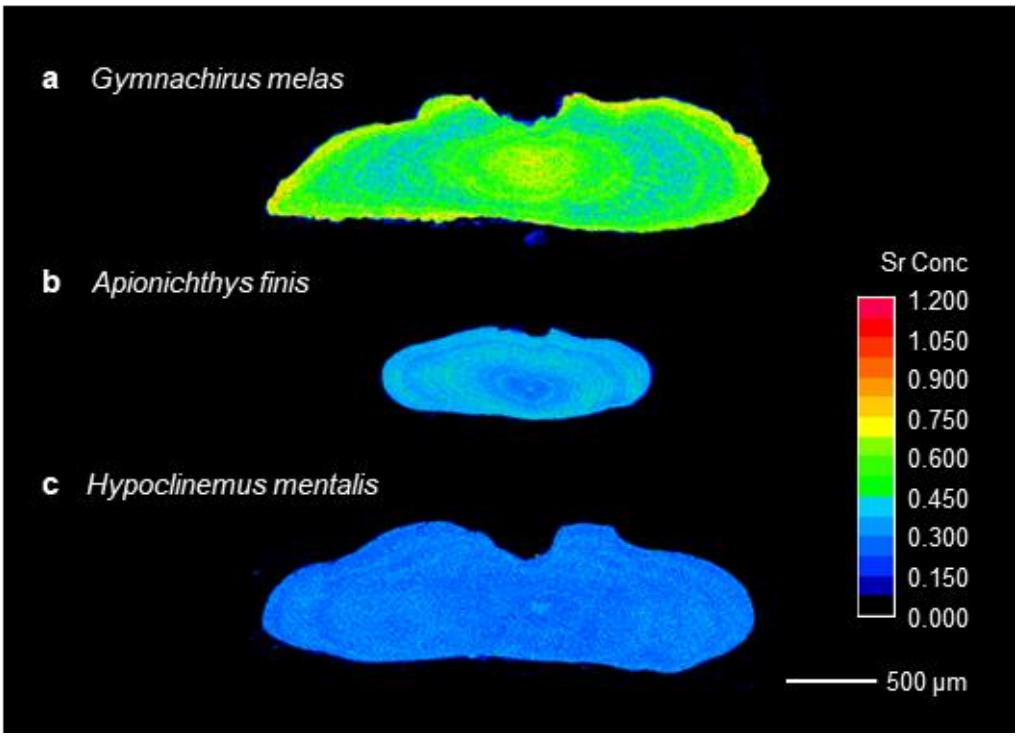
a Gymnachirus melas
b Apionichthys finis
c Hypoclinemus mentalis
Sr Conc
1.200
1.050
0.900
0.750
0.600
0.450
0.300
0.150
0.000
500 µm

Fig. 3

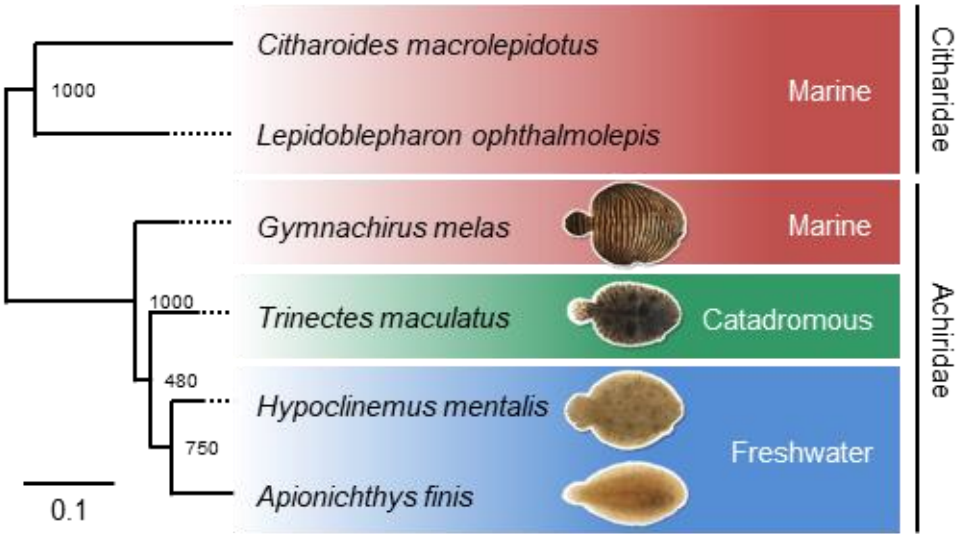
Citharoides macrolepidotus
Lepidoblepharon ophthalmolepis
Marine
Citharidae
1000
Gymnachirus melas
Marine
Trinectes maculatus
Catadromous
Achiridae
1000
480
Hypoclinemus mentalis
750
Freshwater
Apionichthys finis
0.1

Fig. 4

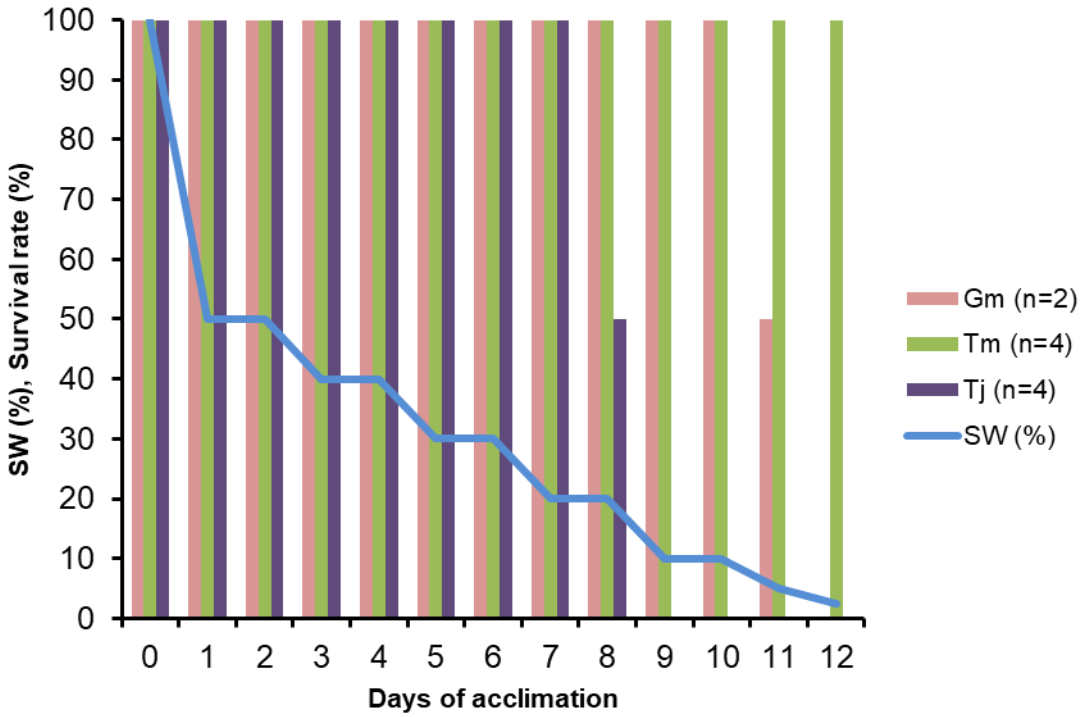
100
90
80
70
60
50
40
30
20
10
0
SW (%), Survival rate (%)
0 1 2 3 4 5 6 7 8 9 10 11 12
Days of acclimation
Gm (n=2)
Tm (n=4)
Tj (n=4)
SW (%)

Fig. 5

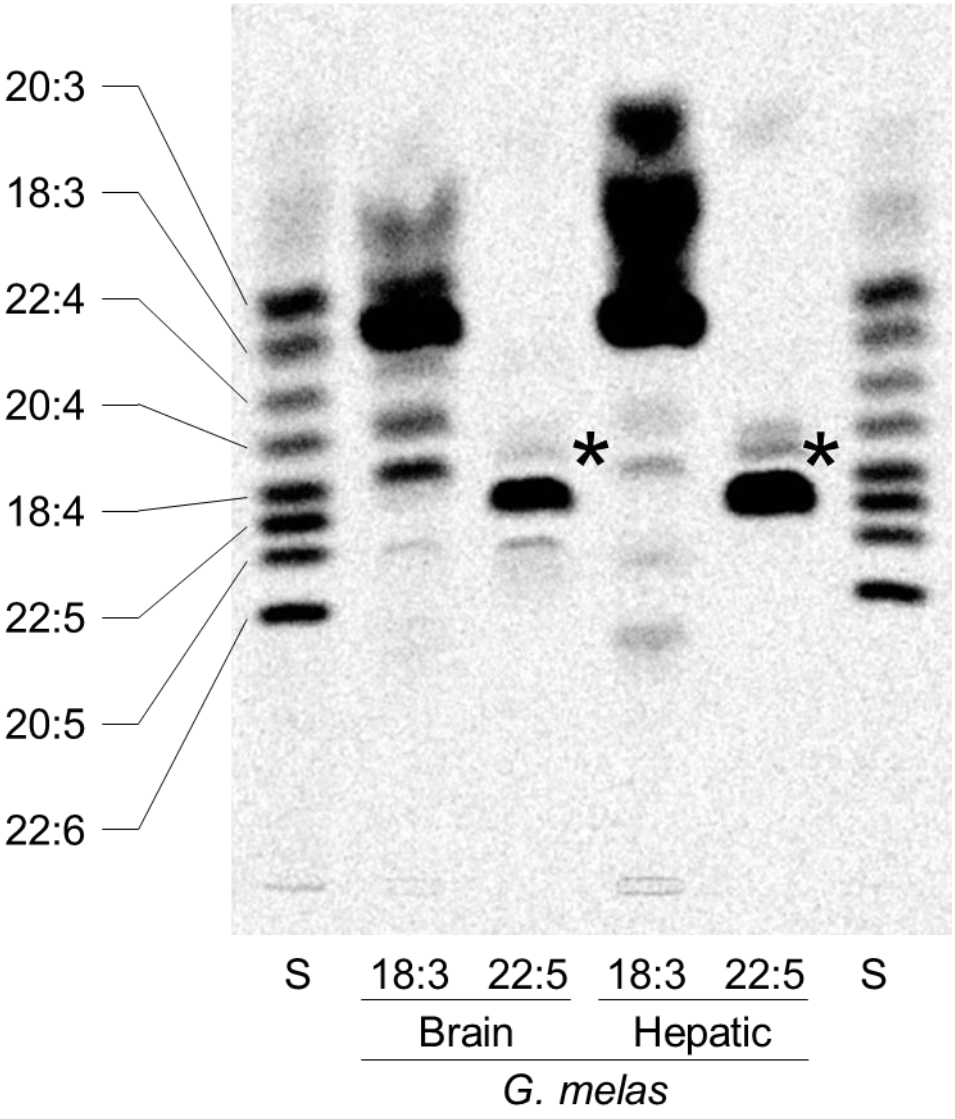
20:3
18:3
22:4
20:4
18:4
22:5
20:5
22:6
*
*
S
18:3
22:5
18:3
22:5
S
Brain
Hepatic
G. melas

Fig. 6

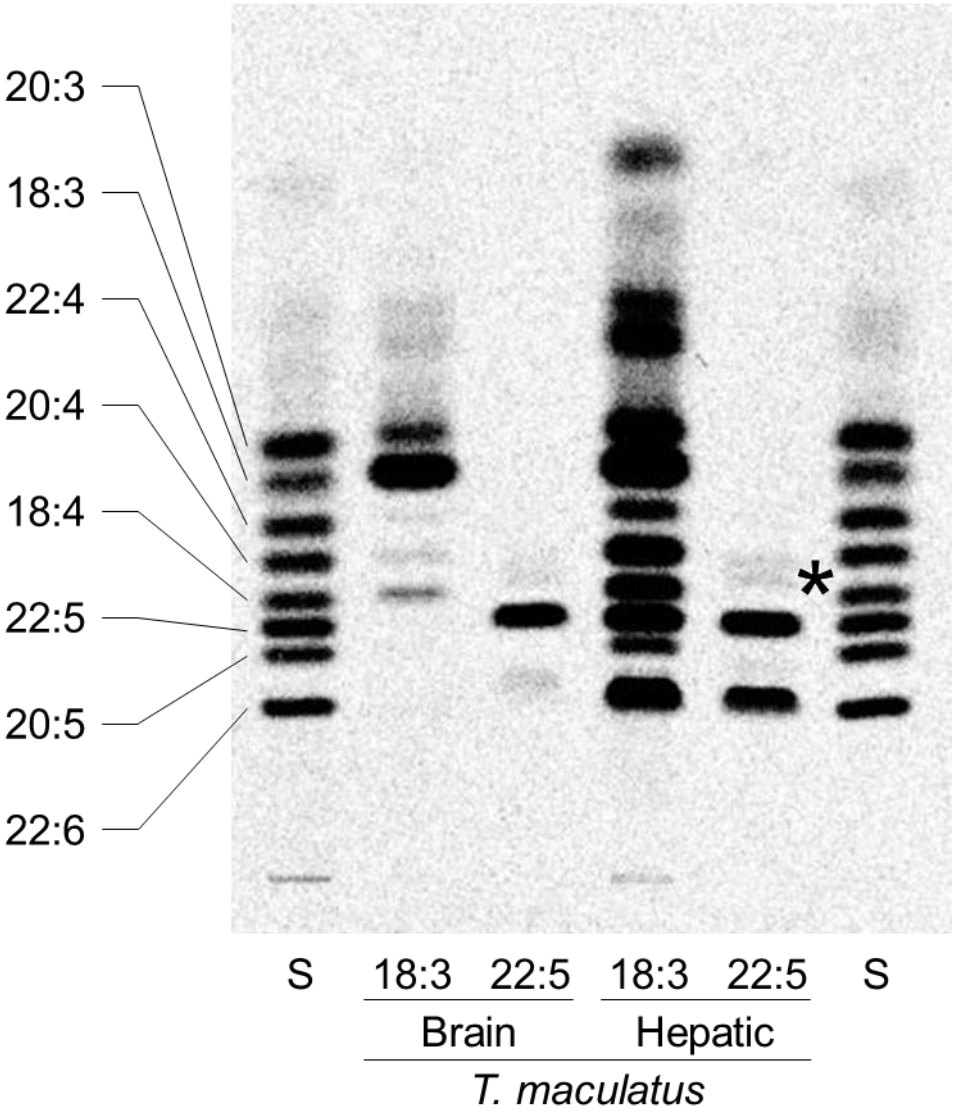
20:3
18:3
22:4
20:4
18:4
22:5
20:5
22:6
*
S
18:3
22:5
18:3
22:5
S
Brain
Hepatic
T. maculatus

Fig. 7

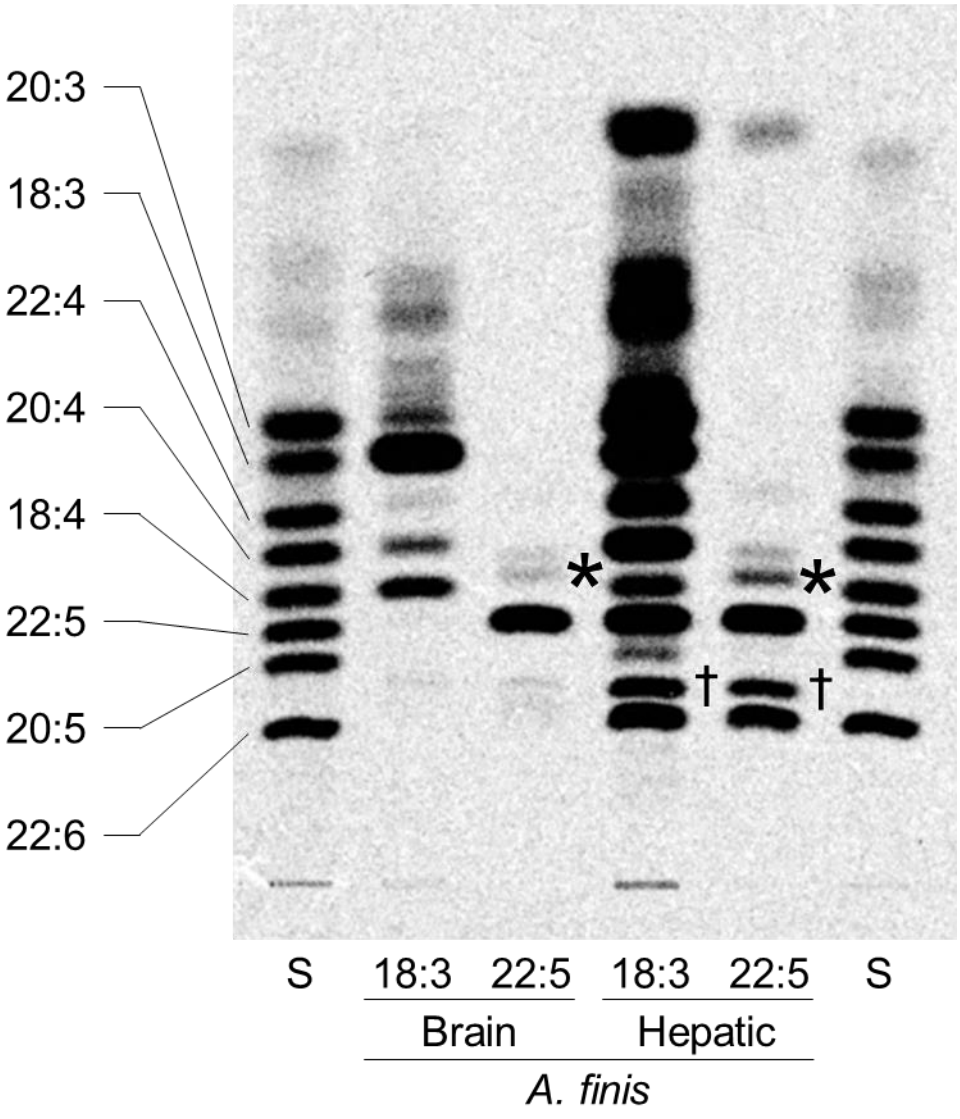
20:3
18:3
22:4
20:4
18:4
22:5
20:5
22:6
*
*
†
†
S
18:3
22:5
18:3
22:5
S
Brain
Hepatic
A. finis

Fig. 8

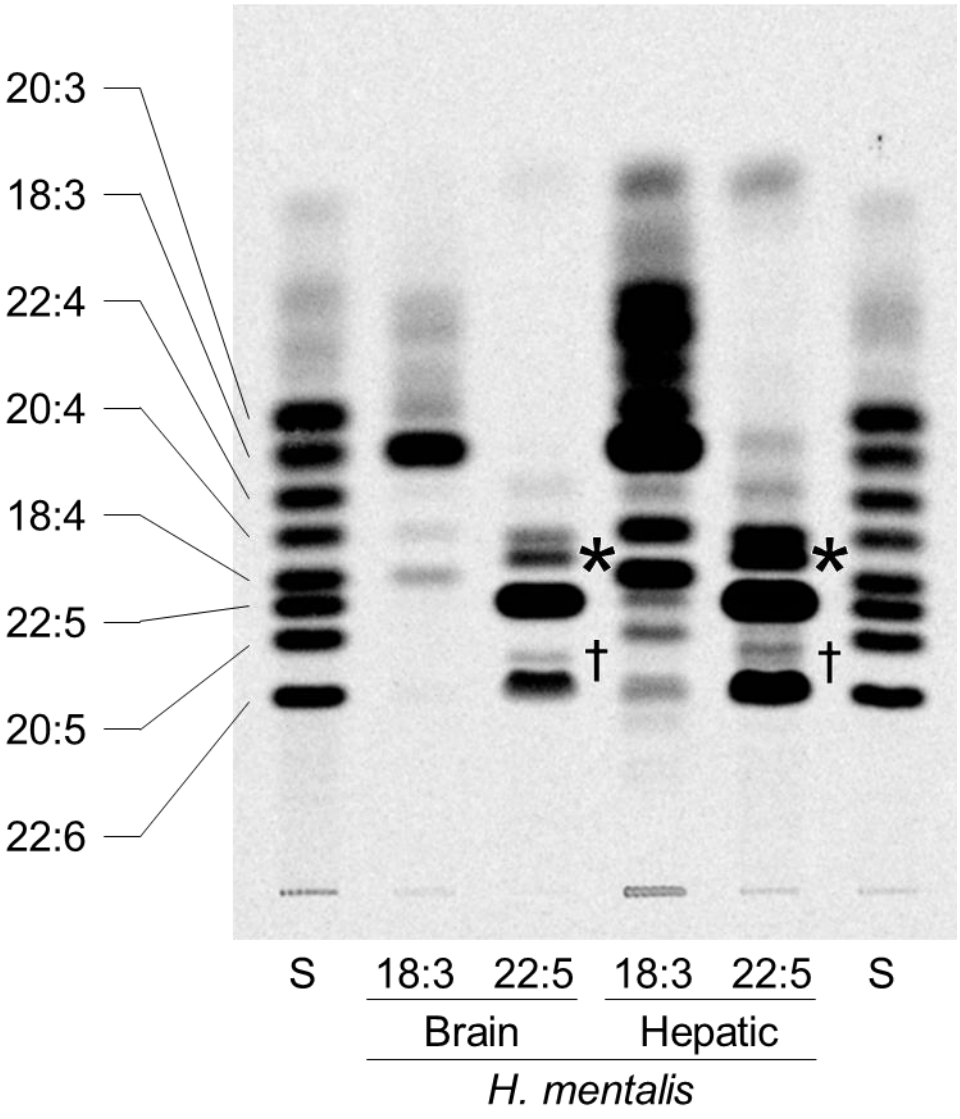
20:3
18:3
22:4
20:4
18:4
22:5
20:5
22:6
*
†
*
†
S
18:3
22:5
18:3
22:5
S
Brain
Hepatic
H. mentalis

Fig. 9

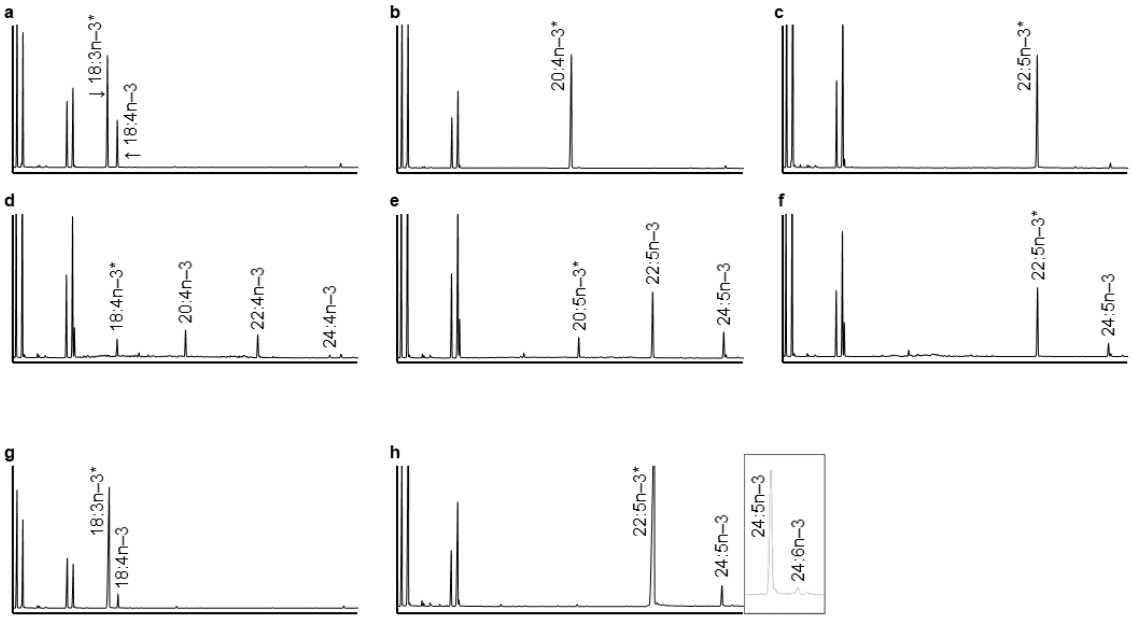
a
18:3n–3*
18:4n–3
b
20:4n–3*
c
22:5n–3*
d
18:4n–3*
20:4n–3
22:4n–3
24:4n–3
e
20:5n–3*
22:5n–3
24:5n–3
f
22:5n–3*
24:5n–3
g
18:3n–3*
18:4n–3
h
22:5n–3*
24:5n–3
24:5n–3
24:6n–3

Fig. 10

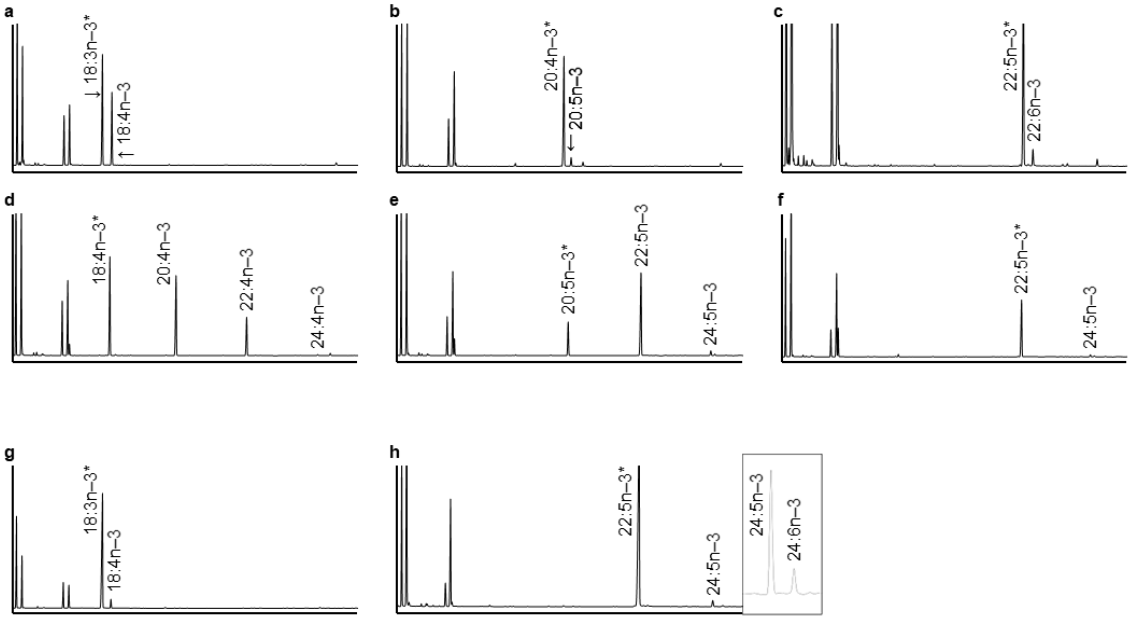
a
18:3n−3*
18:4n−3
b
20:4n−3*
20:5n−3
c
22:5n−3*
22:6n−3
d
18:4n−3*
20:4n−3
22:4n−3
24:4n−3
e
20:5n−3*
22:5n−3
24:5n−3
f
22:5n−3*
24:5n−3
g
18:3n−3*
18:4n−3
h
22:5n−3*
24:5n−3
24:5n−3
24:6n−3

Fig. 11

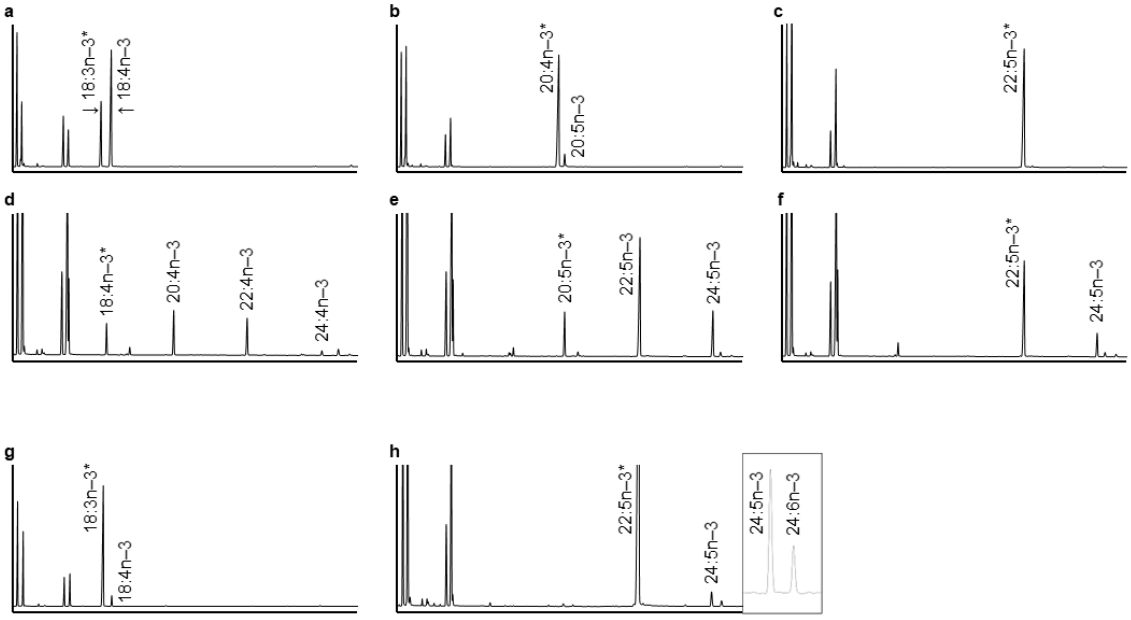
a
18:3n−3*
18:4n−3
b
20:4n−3*
20:5n−3
c
22:5n−3*
d
18:4n−3*
20:4n−3
22:4n−3
24:4n−3
e
20:5n−3*
22:5n−3
24:5n−3
f
22:5n−3*
24:5n−3
g
18:3n−3*
18:4n−3
h
22:5n−3*
24:5n−3
24:5n−3
24:6n−3

Fig. 12

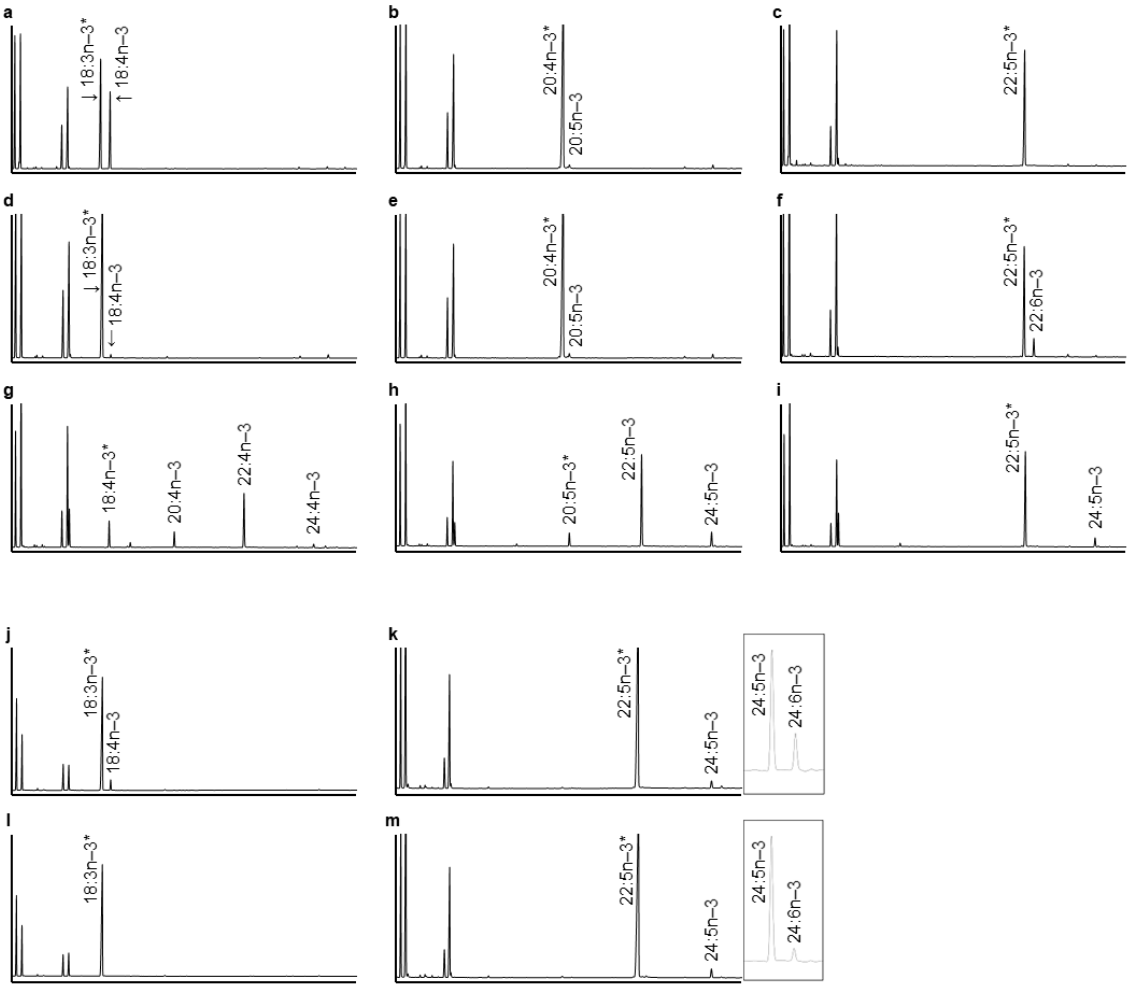
a
18:3n–3*
18:4n–3
b
20:4n–3*
20:5n–3
c
22:5n–3*
d
18:3n–3*
18:4n–3
e
20:4n–3*
20:5n–3
f
22:5n–3*
22:6n–3
g
18:4n–3*
20:4n–3
22:4n–3
24:4n–3
h
20:5n–3*
22:5n–3
24:5n–3
i
22:5n–3*
24:5n–3
j
18:3n–3*
18:4n–3
k
22:5n–3*
24:5n–3
24:5n–3
24:6n–3
l
18:3n–3*
m
22:5n–3*
24:5n–3
24:5n–3
24:6n–3

Fig. 13

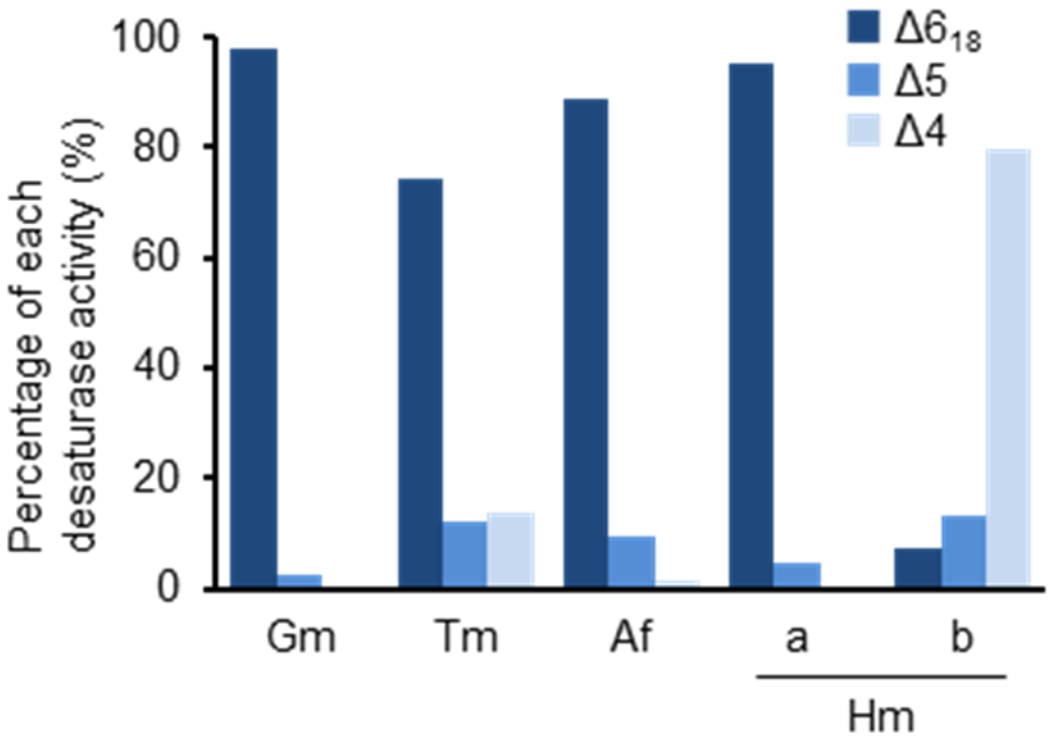
Percentage of each desaturase activity (%)
100
80
60
40
20
0
Δ6₁₈
Δ5
Δ4
Gm
Tm
Af
a
b
Hm

Fig. 14

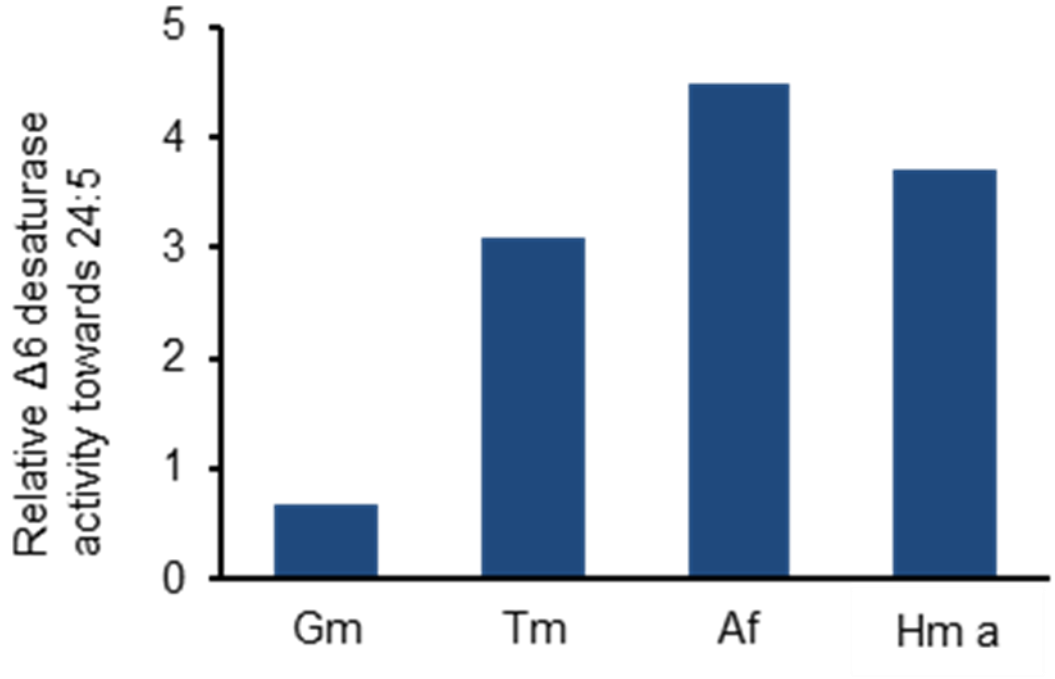
Relative Δ6 desaturase activity towards 24:5
5
4
3
2
1
0
Gm
Tm
Af
Hm a

Fig. 15

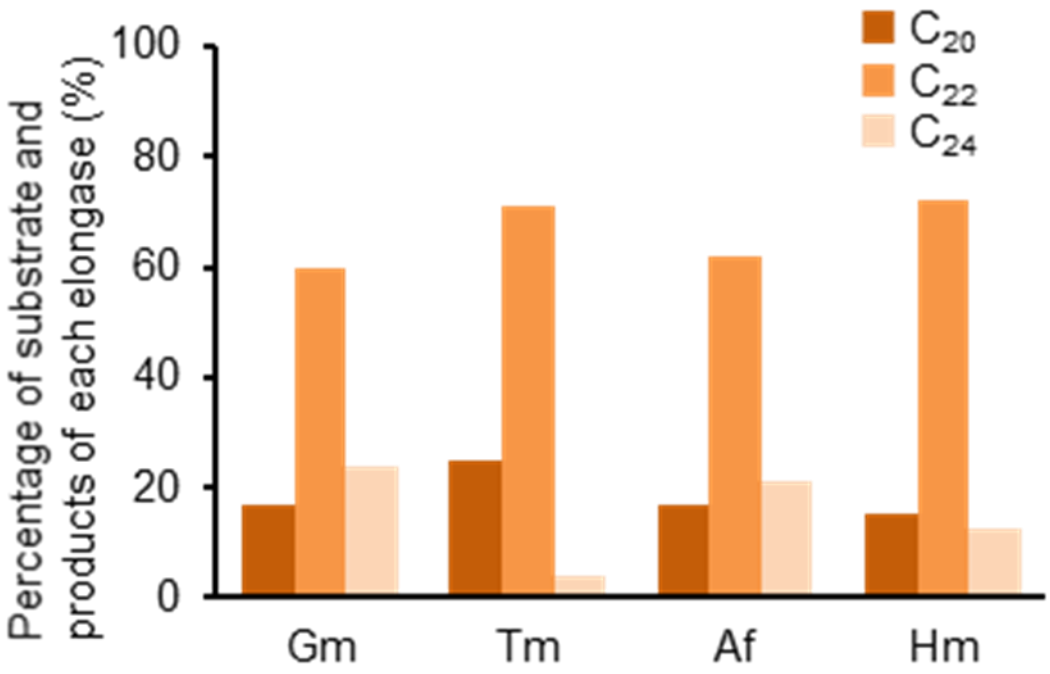
Percentage of substrate and products of each elongase (%)
100
80
60
40
20
0
Gm
Tm
Af
Hm
C20
C22
C24

Fig. 16

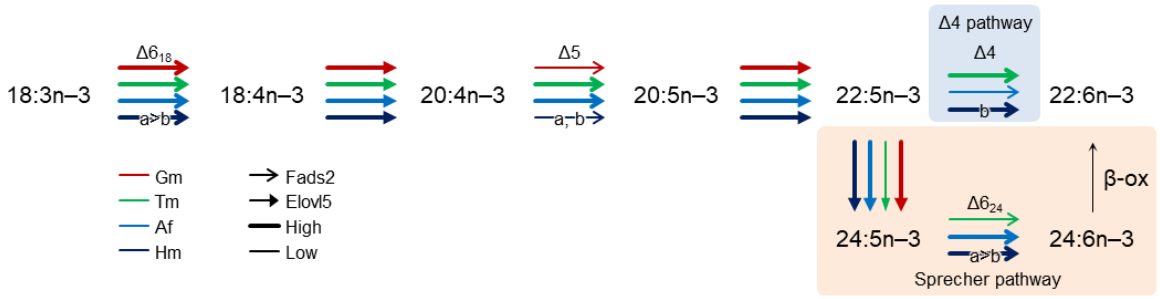
18:3n–3
Δ6₁₈
a>b
18:4n–3
20:4n–3
Δ5
a,–b
20:5n–3
22:5n–3
Δ4 pathway
Δ4
b
22:6n–3
β-ox
24:5n–3
Δ6₂₄
a>b
24:6n–3
Sprecher pathway
Gm
Tm
Af
Hm
Fads2
Elovl5
High
Low

Fig. 17

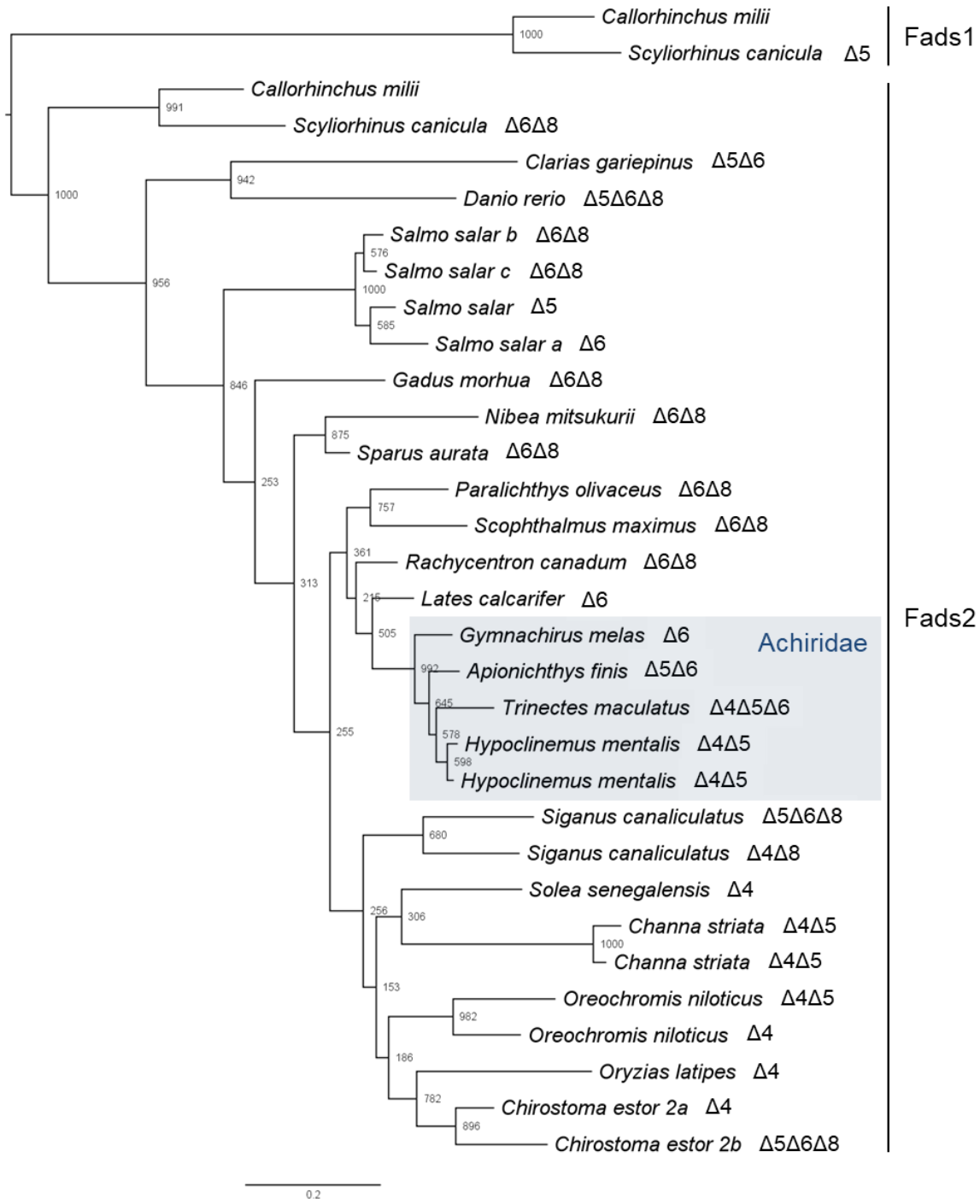
Callorhinchus milii
Scyliorhinus canicula Δ5
Fads1
Callorhinchus milii
Scyliorhinus canicula Δ6Δ8
Clarias gariepinus Δ5Δ6
Danio rerio Δ5Δ6Δ8
Salmo salar b Δ6Δ8
Salmo salar c Δ6Δ8
Salmo salar Δ5
Salmo salar a Δ6
Gadus morhua Δ6Δ8
Nibea mitsukurii Δ6Δ8
Sparus aurata Δ6Δ8
Paralichthys olivaceus Δ6Δ8
Scophthalmus maximus Δ6Δ8
Rachycentron canadum Δ6Δ8
Lates calcarifer Δ6
Gymnachirus melas Δ6
Achiridae
Apionichthys finis Δ5Δ6
Trinectes maculatus Δ4Δ5Δ6
Hypoclinemus mentalis Δ4Δ5
Hypoclinemus mentalis Δ4Δ5
Siganus canaliculatus Δ5Δ6Δ8
Siganus canaliculatus Δ4Δ8
Solea senegalensis Δ4
Channa striata Δ4Δ5
Channa striata Δ4Δ5
Oreochromis niloticus Δ4Δ5
Oreochromis niloticus Δ4
Oryzias latipes Δ4
Chirostoma estor 2a Δ4
Chirostoma estor 2b Δ5Δ6Δ8
Fads2
0.2

Fig. 18

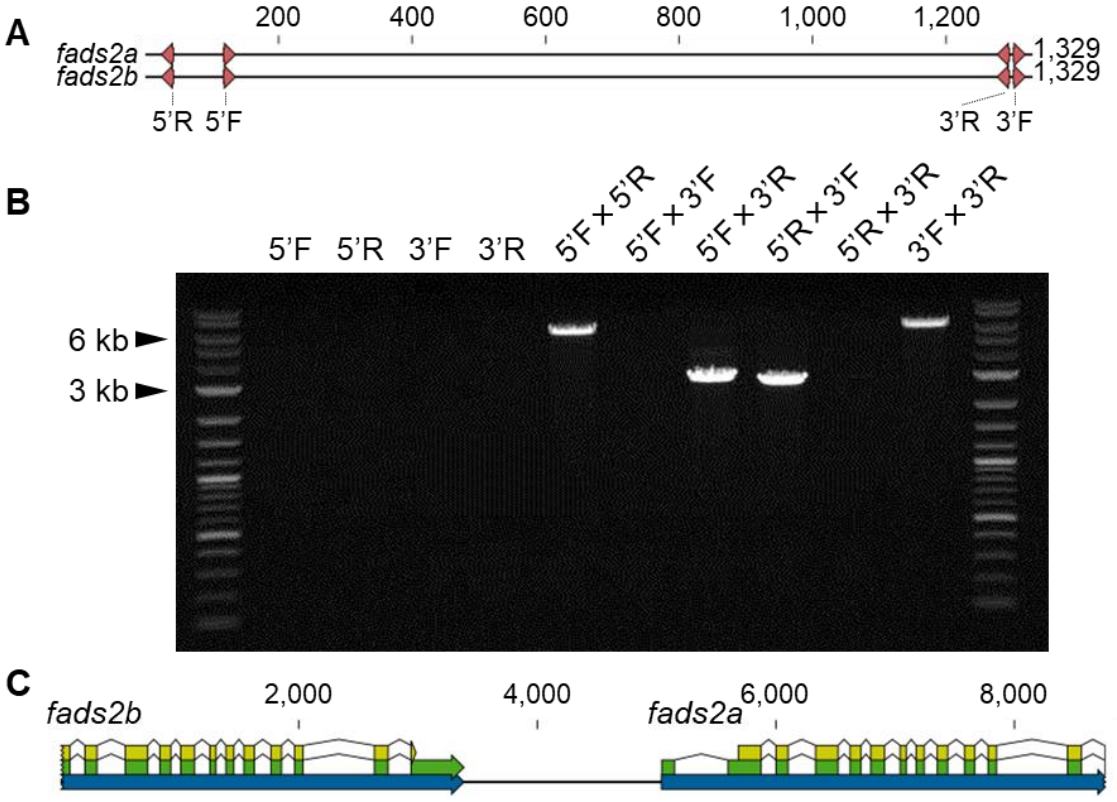
A
200
400
600
800
1,000
1,200
fads2a
fads2b
1,329
1,329
5'R 5'F
3'R 3'F
B
5'F
5'R
3'F
3'R
5'F×5'R
5'F×3'F
5'F×3'R
5'R×3'F
5'R×3'R
3'F×3'R
6 kb
3 kb
C
fads2b
2,000
4,000
fads2a
6,000
8,000

Fig. 19

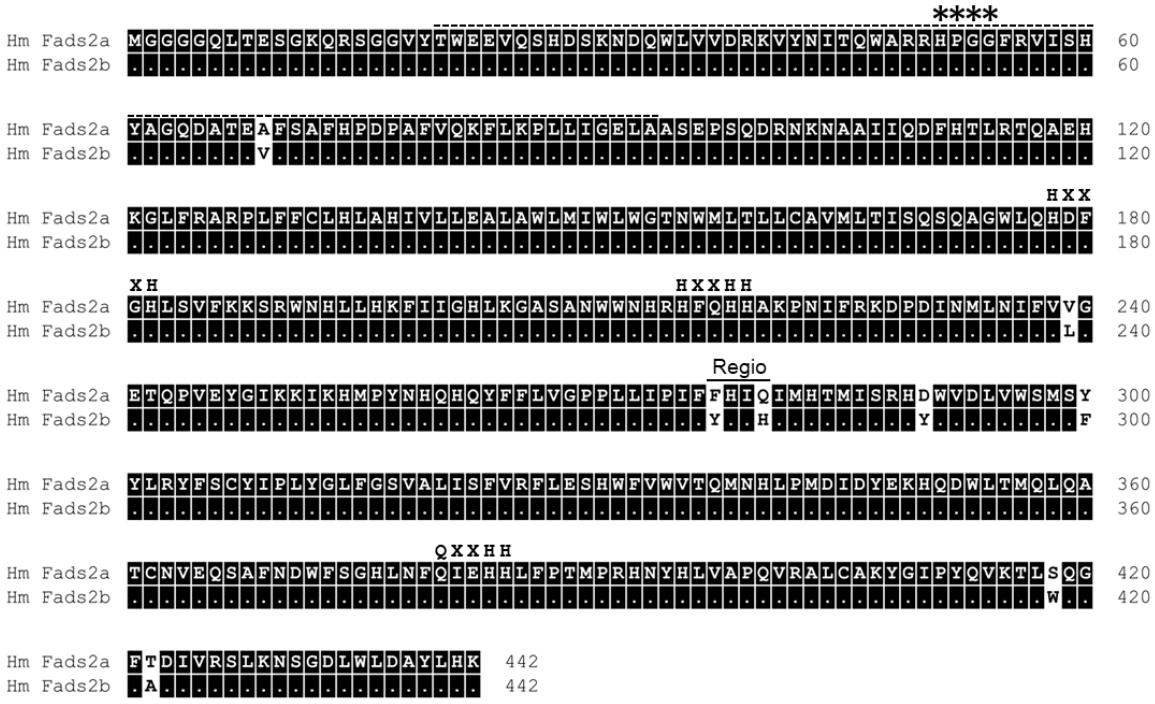
****
Hm Fads2a MGGGGQLTESGKQRSGGVYTWEEVQSHDSKNDQWLVVDRKVYNITQWARRHPGGFRVISH 60
Hm Fads2b 60
Hm Fads2a YAGQDATEAFSAFHPDPAFVQKFLKPLLIGELAASEPSQDRNKNAAIIQDFHTLRTQAEH 120
Hm Fads2b .....V..... 120
HXX
Hm Fads2a KGLFRARPLFFCLHLAHIVLLEALAWLMIWLWGTNWMLTLLCAVMLTISQSQAGWLQHDF 180
Hm Fads2b 180
XH
HXXHH
Hm Fads2a GHLSVFKKSRWNHLLHKFIIGHLKGASANWWNHRHFQHHAKPNIFRKDPDINMLNIFVVG 240
Hm Fads2b .....L. 240
Regio
Hm Fads2a ETQPVEYGIKKIKHMPYNHQHQYFFLVGPPLLIPIFFHIQIMHTMISRHDWVDLVWSMSY 300
Hm Fads2b .....Y..H.....Y.....F 300
Hm Fads2a YLRYFSCYIPLYGLFGSVALISFVRFLESHWFVWVTQMNHLPMDIDYEKHQDWLTMQLQA 360
Hm Fads2b 360
QXXHH
Hm Fads2a TCNVEQSAFNDWFSGHLNFQIEHHLFPTMPRHNYHLVAPQVRALCAKYGIPYQVKTLSQG 420
Hm Fads2b .....W.. 420
Hm Fads2a FTDIVRSLKNSGDLWLDAYLHK 442
Hm Fads2b .A..... 442

Fig. 20

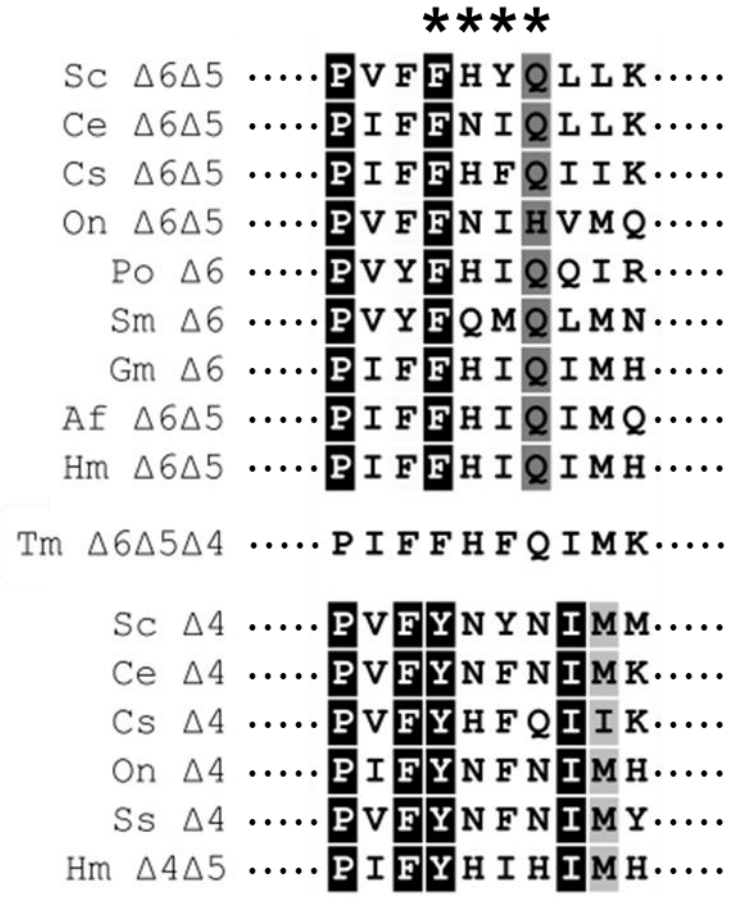
****
Sc Δ6Δ5 .....PVFFHYQLLK.....
Ce Δ6Δ5 .....PIFFNIQLLK.....
Cs Δ6Δ5 .....PIFFHFQIIK.....
On Δ6Δ5 .....PVFFNIHVMQ.....
Po Δ6 .....PVYFHIQQIR.....
Sm Δ6 .....PVYFQMQLMN.....
Gm Δ6 .....PIFFHIQIMH.....
Af Δ6Δ5 .....PIFFHIQIMQ.....
Hm Δ6Δ5 .....PIFFHIQIMH.....
Tm Δ6Δ5Δ4 .....PIFFHFQIMK.....
Sc Δ4 .....PVFYNYNIMM.....
Ce Δ4 .....PVFYNFNIMK.....
Cs Δ4 .....PVFYHFQIIK.....
On Δ4 .....PIFYNFNIMH.....
Ss Δ4 .....PVFYNFNIMY.....
Hm Δ4Δ5 .....PIFYHIHIMH.....

Fig. 21

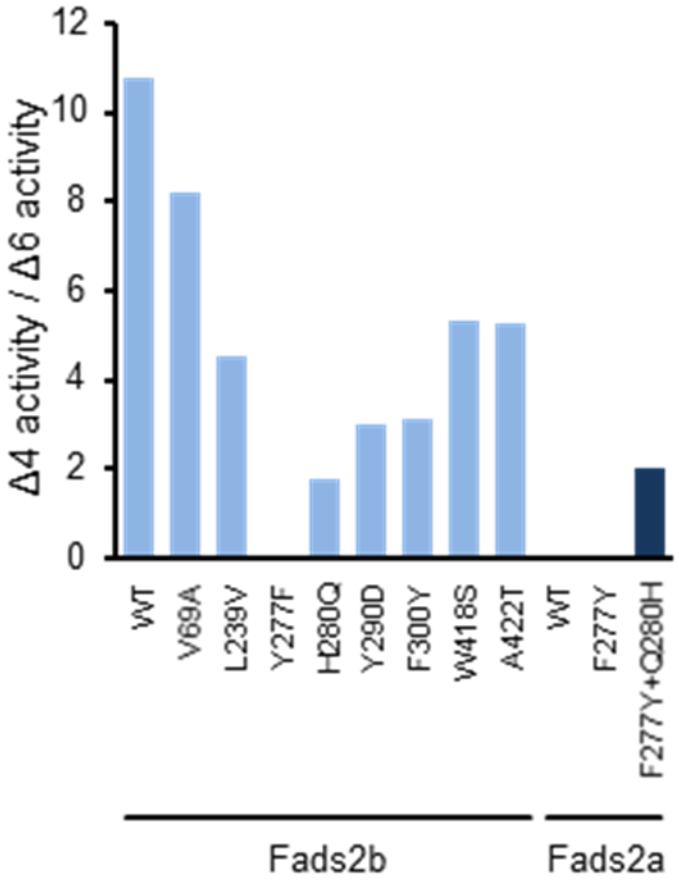
Δ4 activity / Δ6 activity
0
2
4
6
8
10
12
WT
V69A
L239V
Y277F
H280Q
Y290D
F300Y
W418S
A422T
WT
F277Y
F277Y+Q280H
Fads2b
Fads2a

Fig. 22

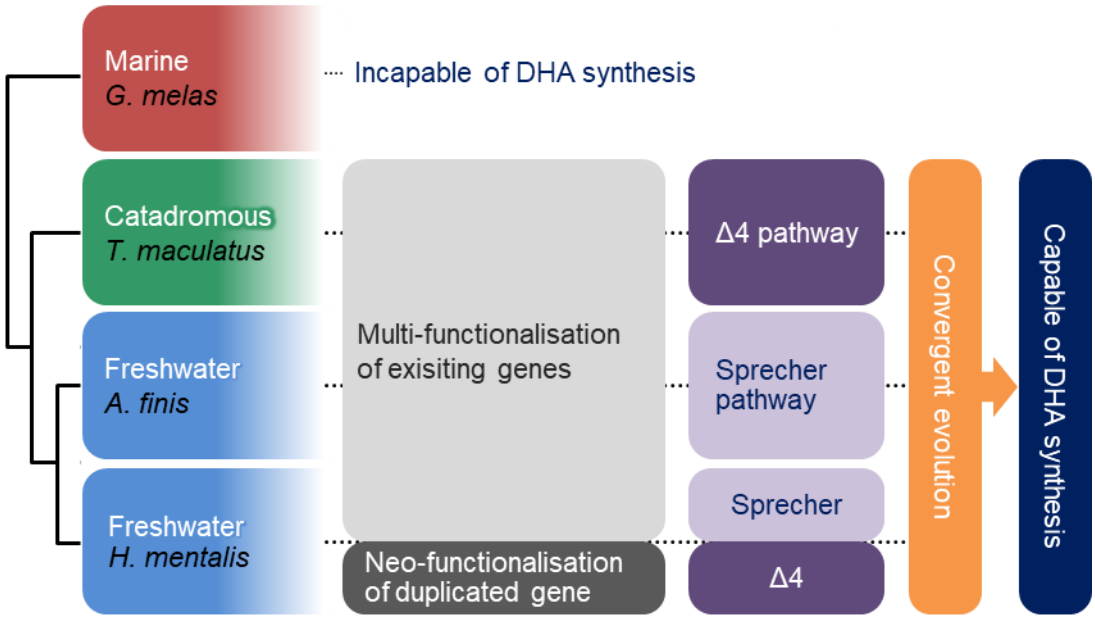
Marine
G. melas
Incapable of DHA synthesis
Catadromous
T. maculatus
Freshwater
A. finis
Freshwater
H. mentalis
Multi-functionalisation
of exisiting genes
Neo-functionalisation
of duplicated gene
Δ4 pathway
Sprecher
pathway
Sprecher
Δ4
Convergent evolution
Capable of DHA synthesis

Fig. 23

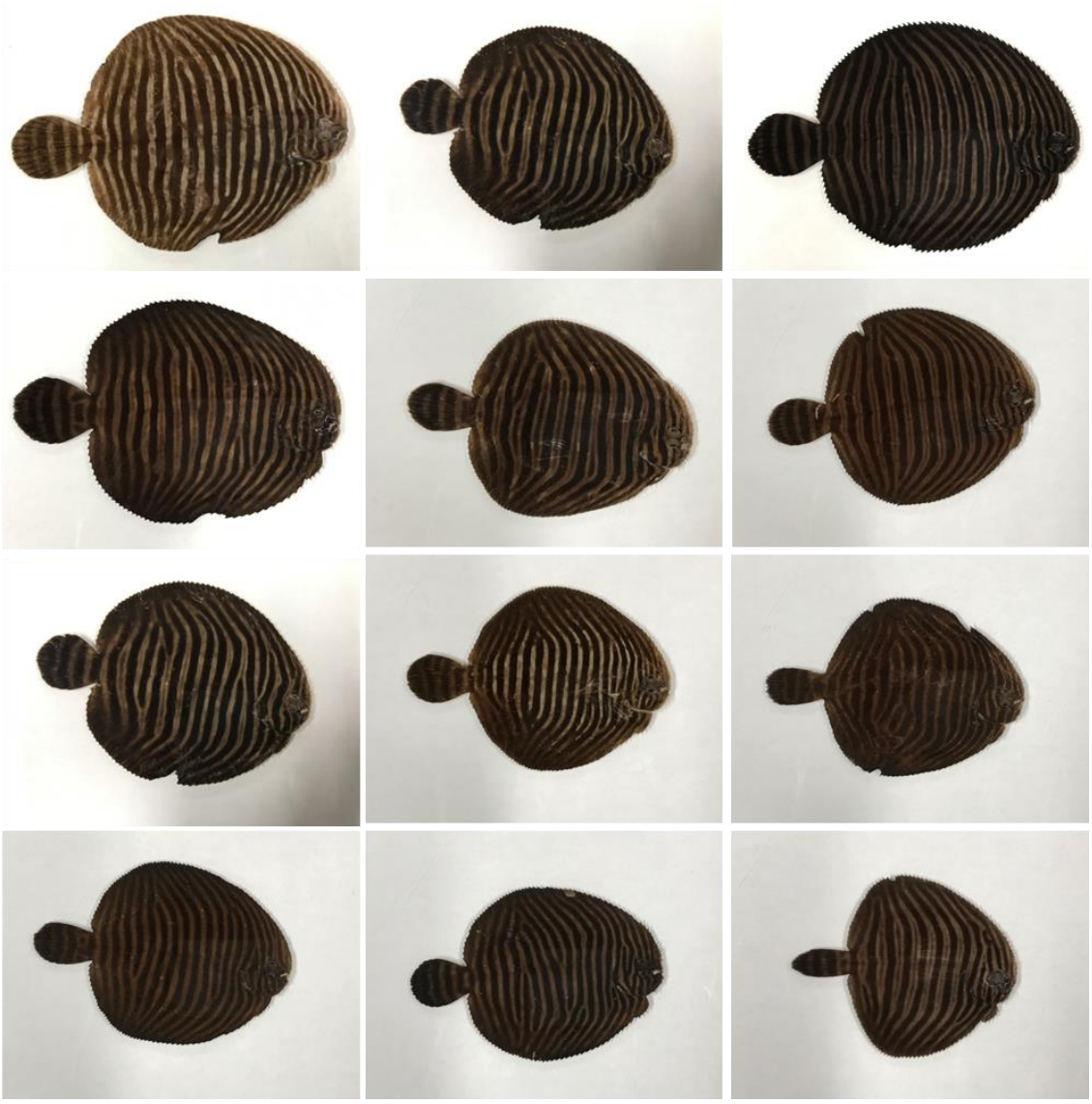

Fig. 24

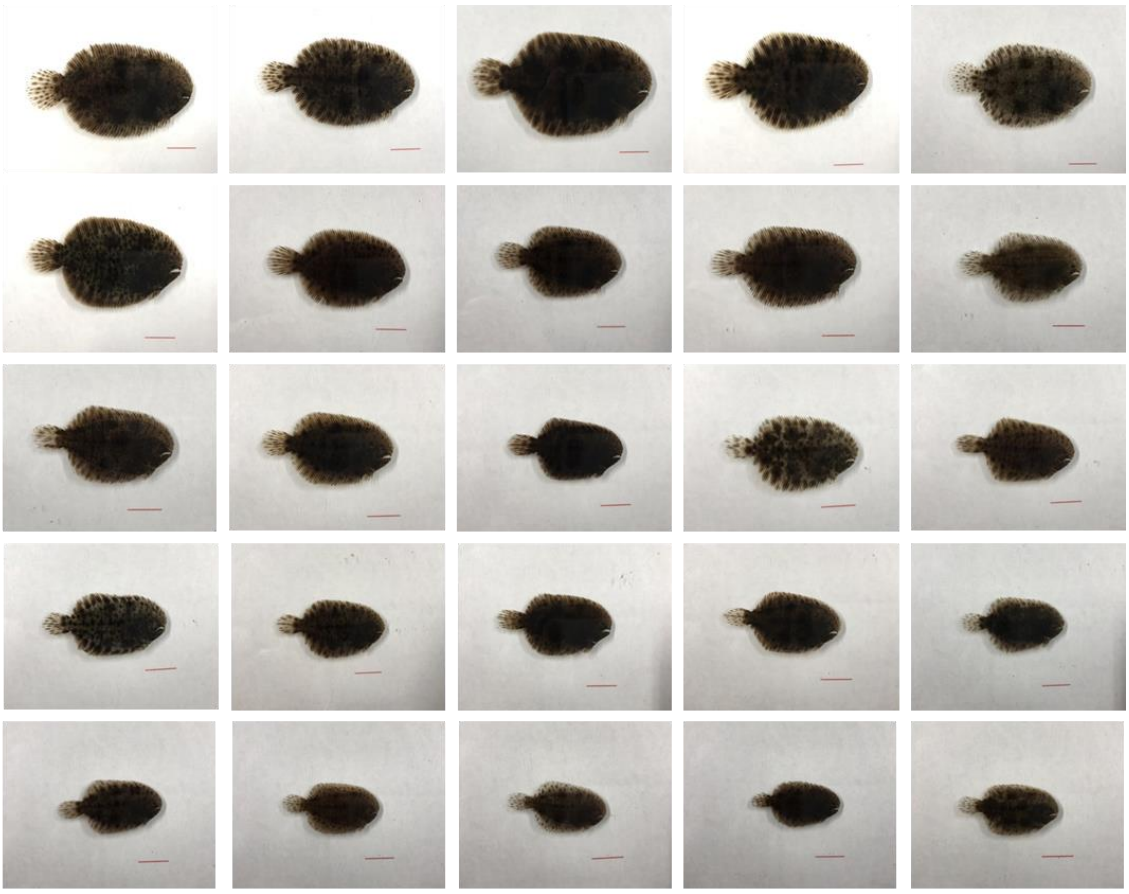

Scale bars = 1 cm

Fig. 25

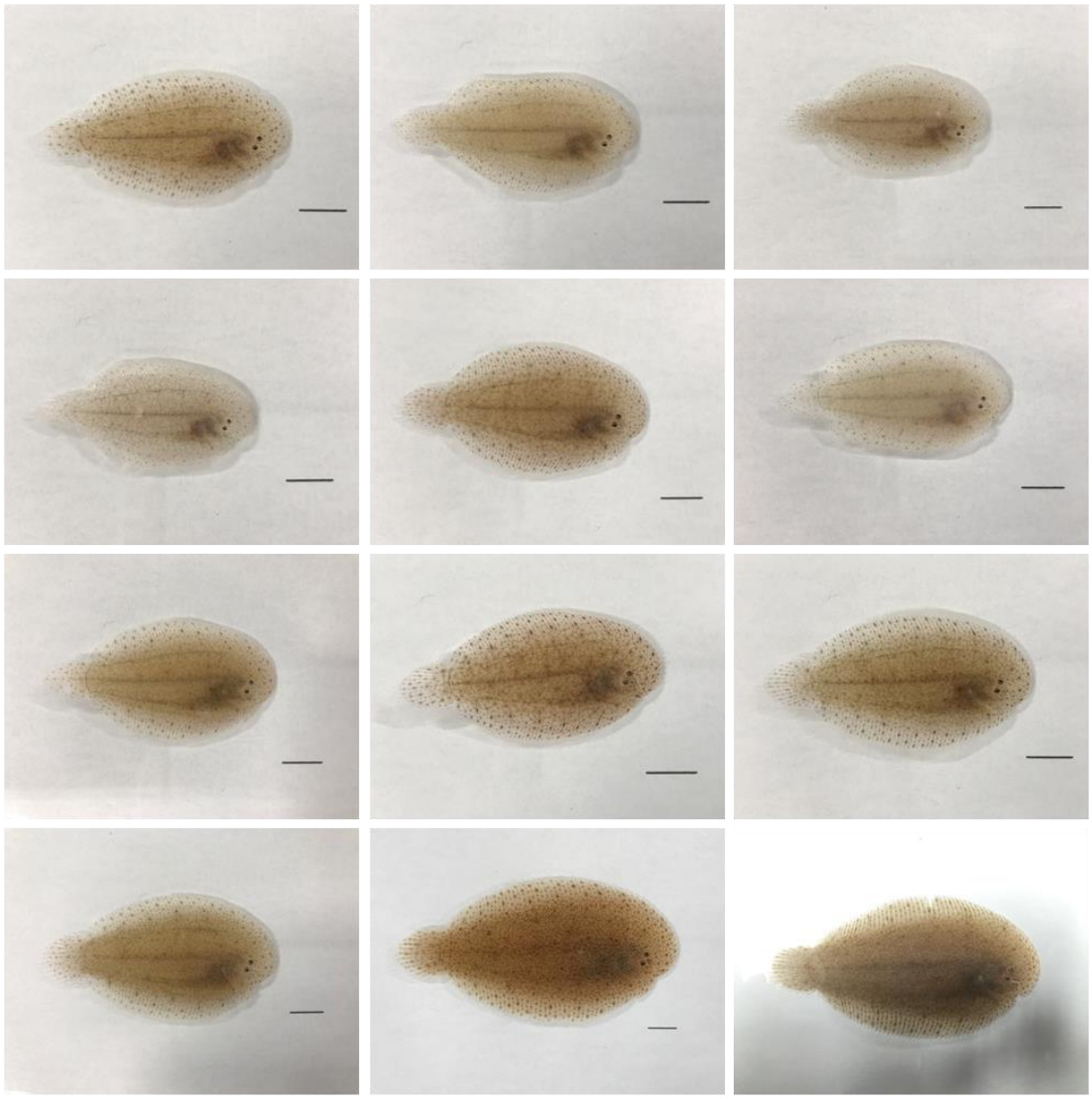

Scale bars = 1 cm

Fig. 26

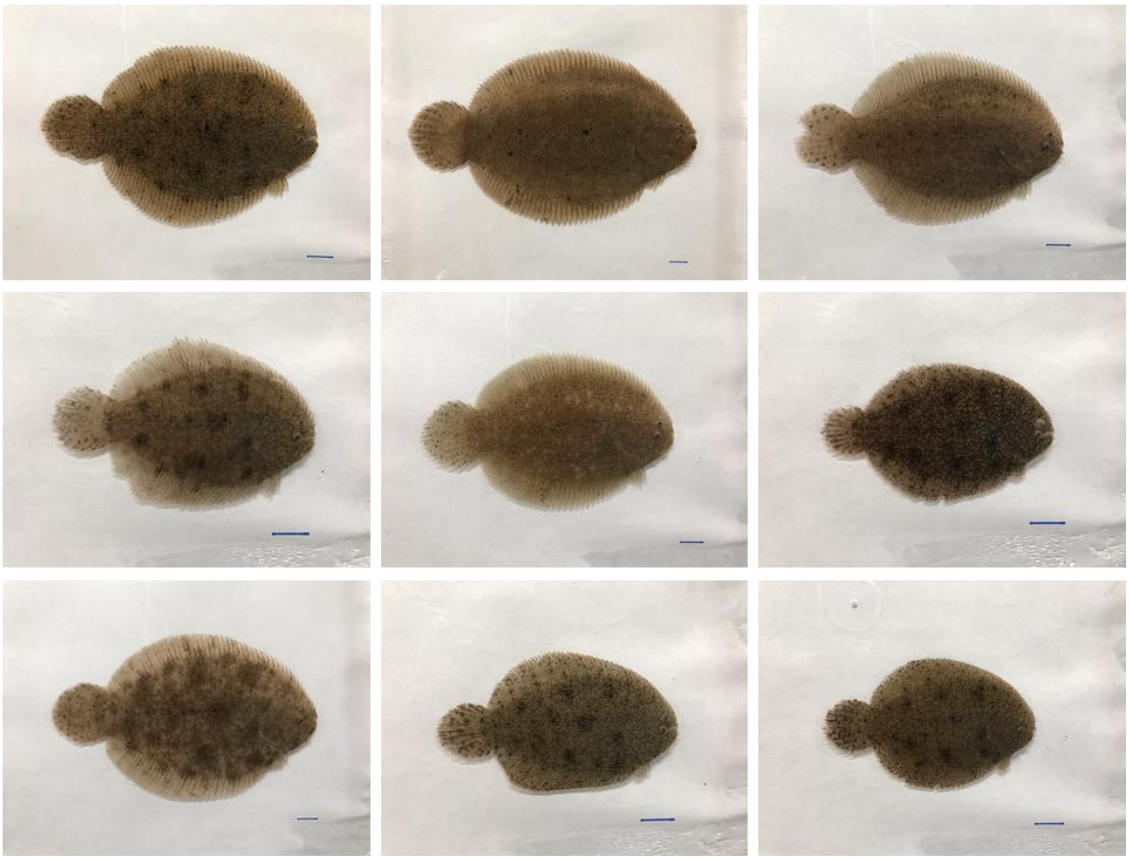

Scale bars = 1 cm

Fig. 27

Gymnachirus melas 16S rRNA gene, partial sequence

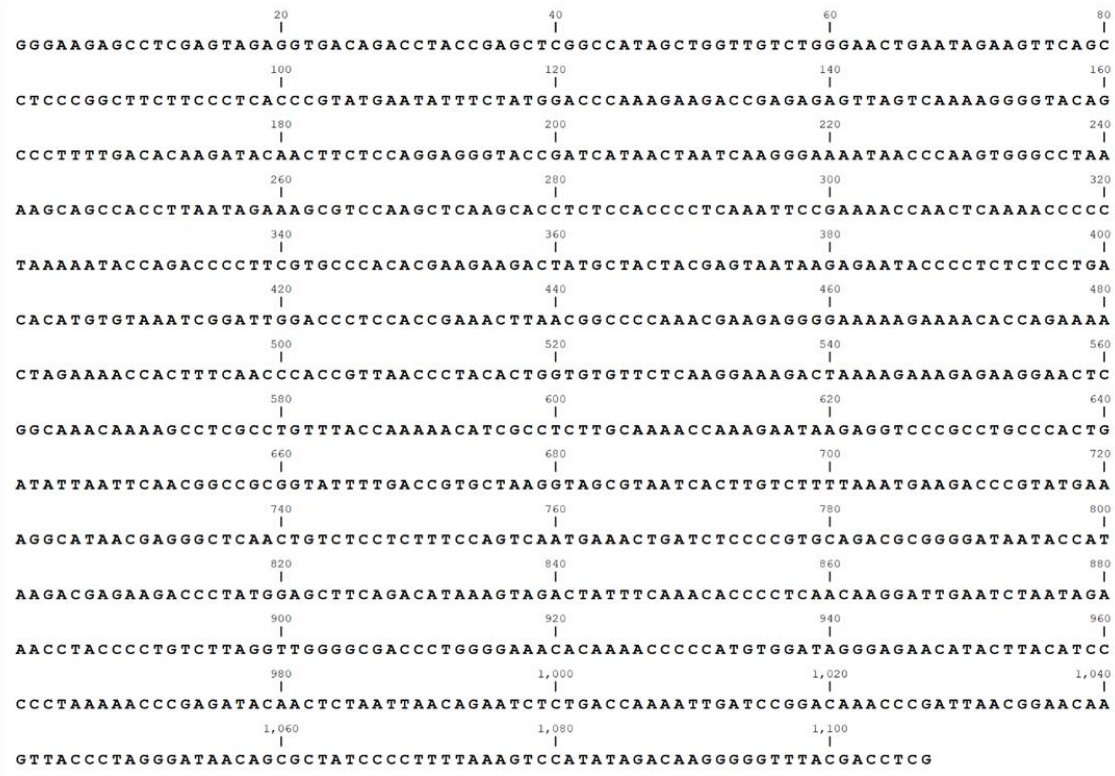

Fig. 28

Trinectes maculatus 16S rRNA gene, partial sequence

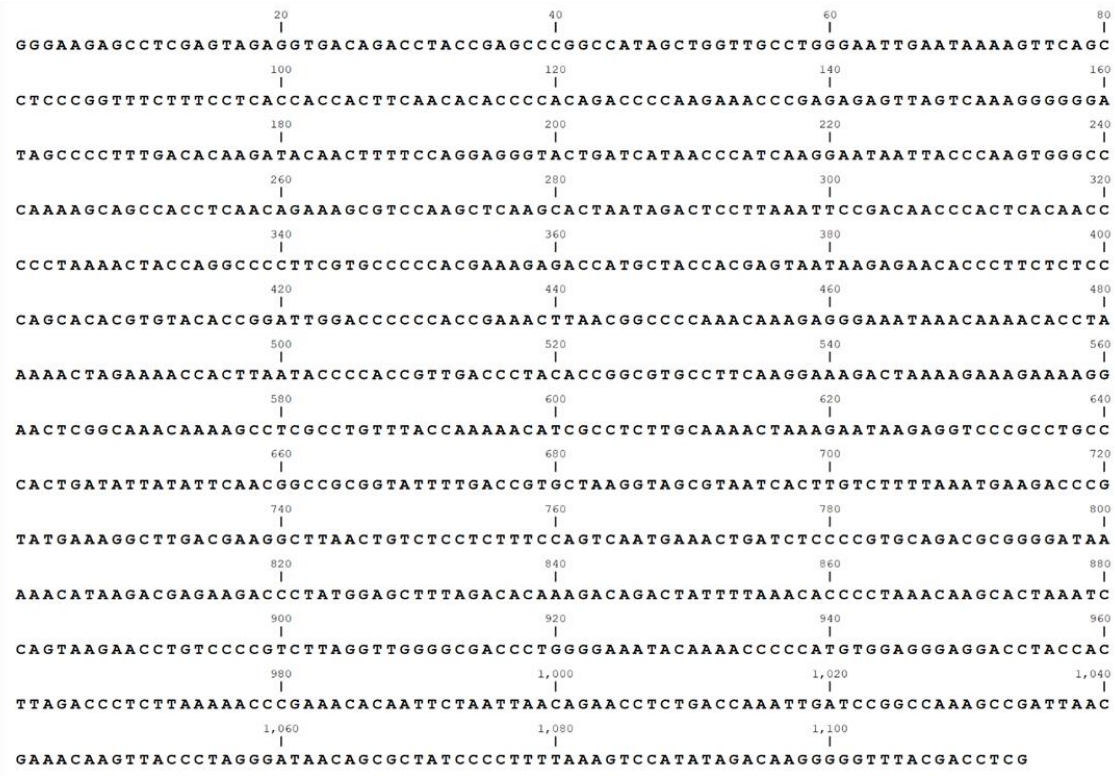

Fig. 29

Apionichthys finis 16S rRNA gene, partial sequence

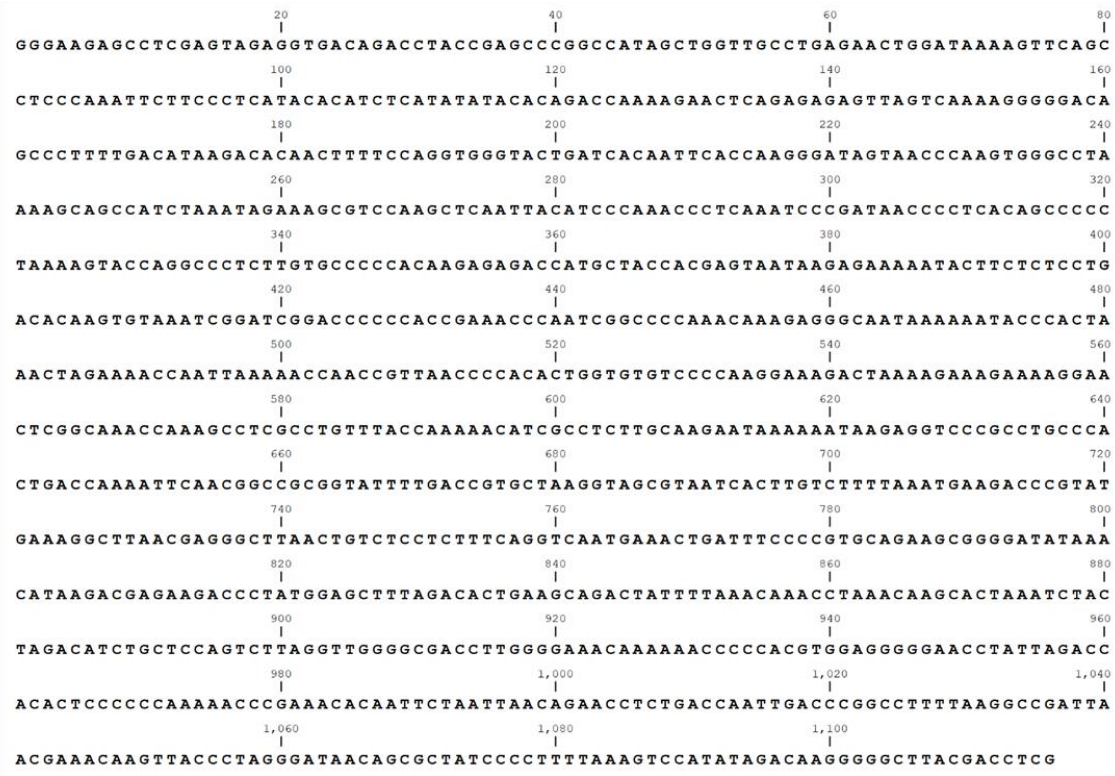

Fig. 30

Hypoclinemus mentalis 16S rRNA gene, partial sequence

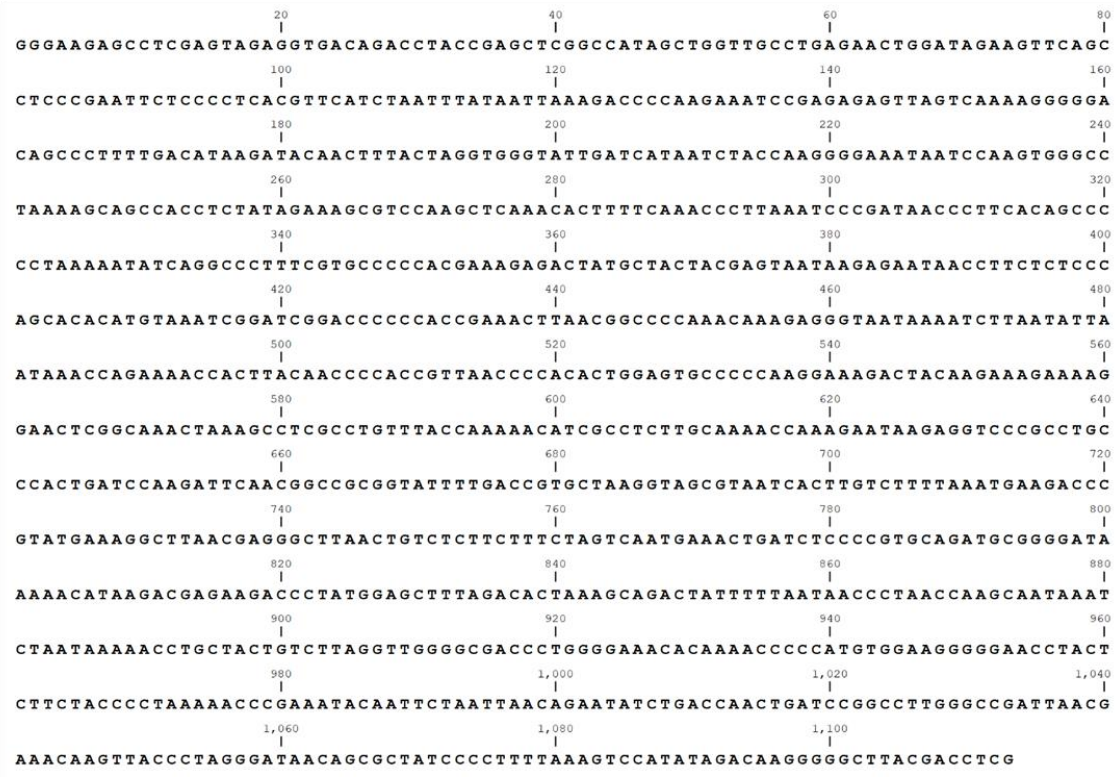

Fig. 31

Gymnachirus melas fads2 mRNA, partial sequence

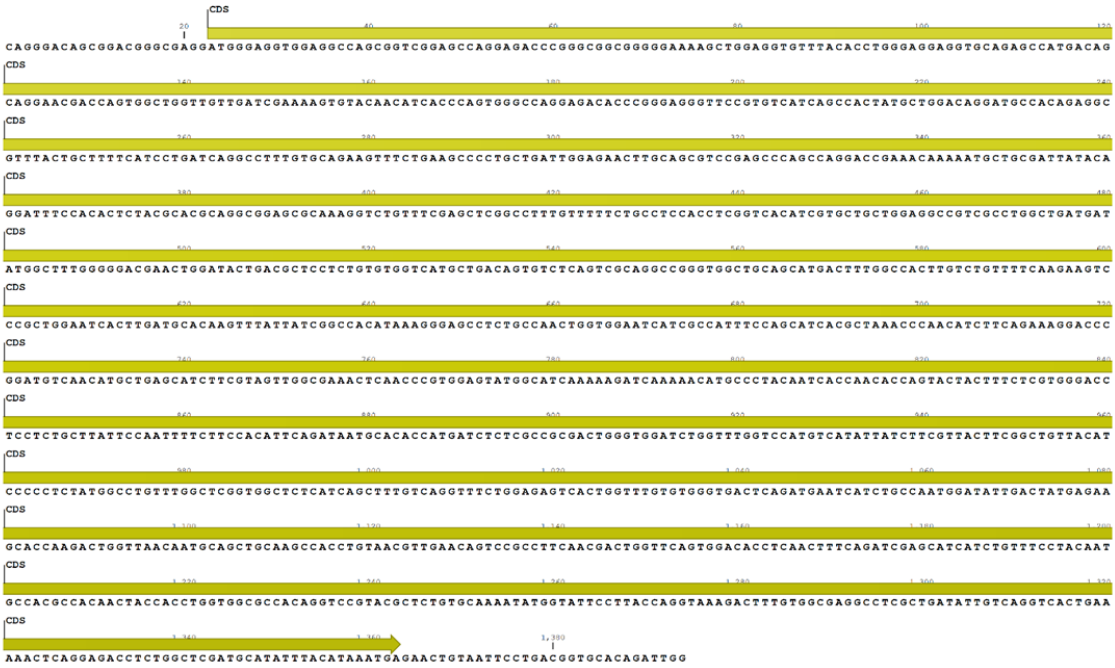

Gymnachirus melas Fads2 amino acid sequence

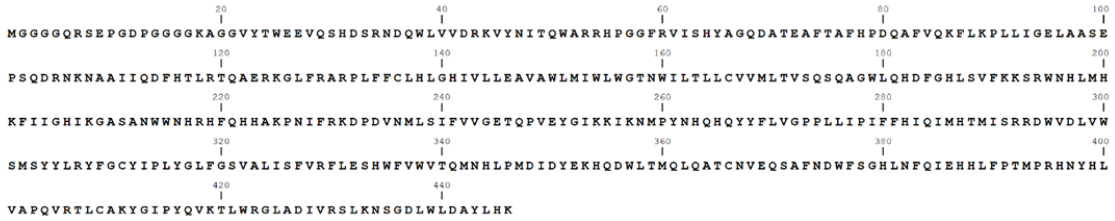

Fig. 32

Trinectes maculatus fads2 mRNA, complete sequence

Trinectes maculatus Fads2 amino acid sequence

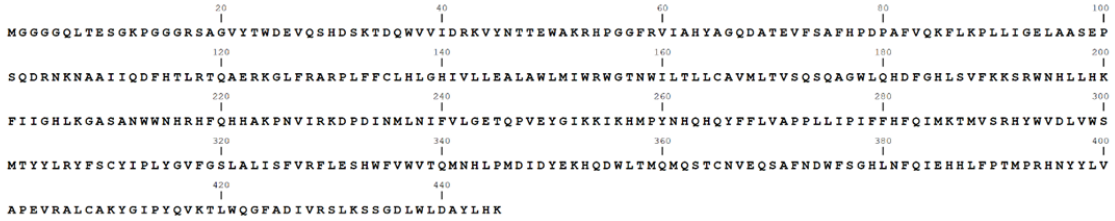

Fig. 33

Apionichthys finis fads2 mRNA, partial sequence

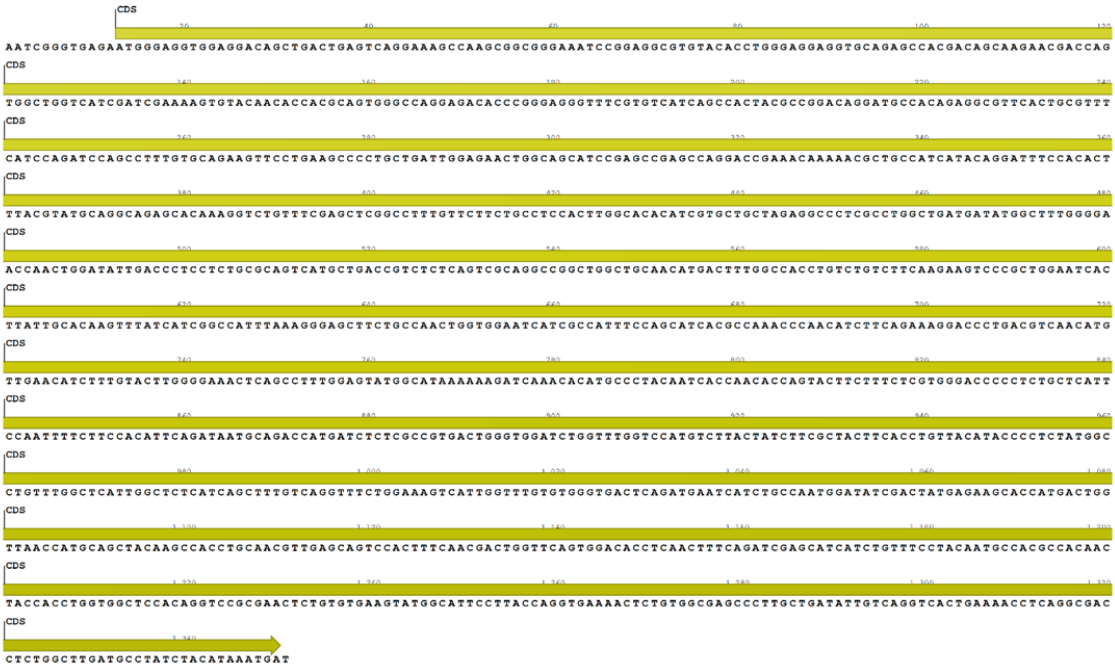

Apionichthys finis Fads2 amino acid sequence

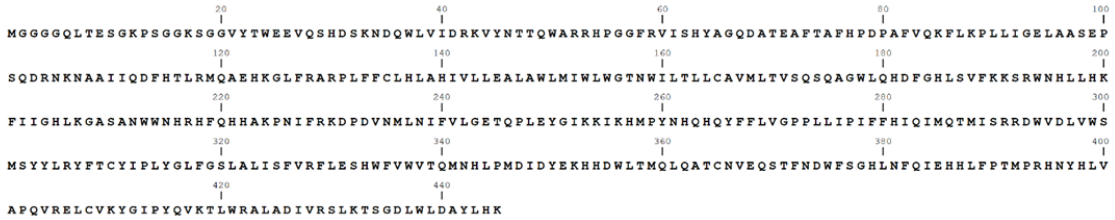

Fig. 34

Hypoclinemus mentalis fads2a mRNA, complete CDS

Hypoclinemus mentalis Fads2a amino acid sequence

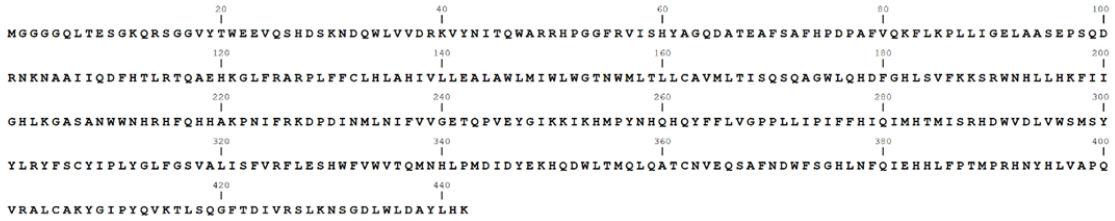

Fig. 35

Hypoclinemus mentalis fads2b mRNA, complete CDS

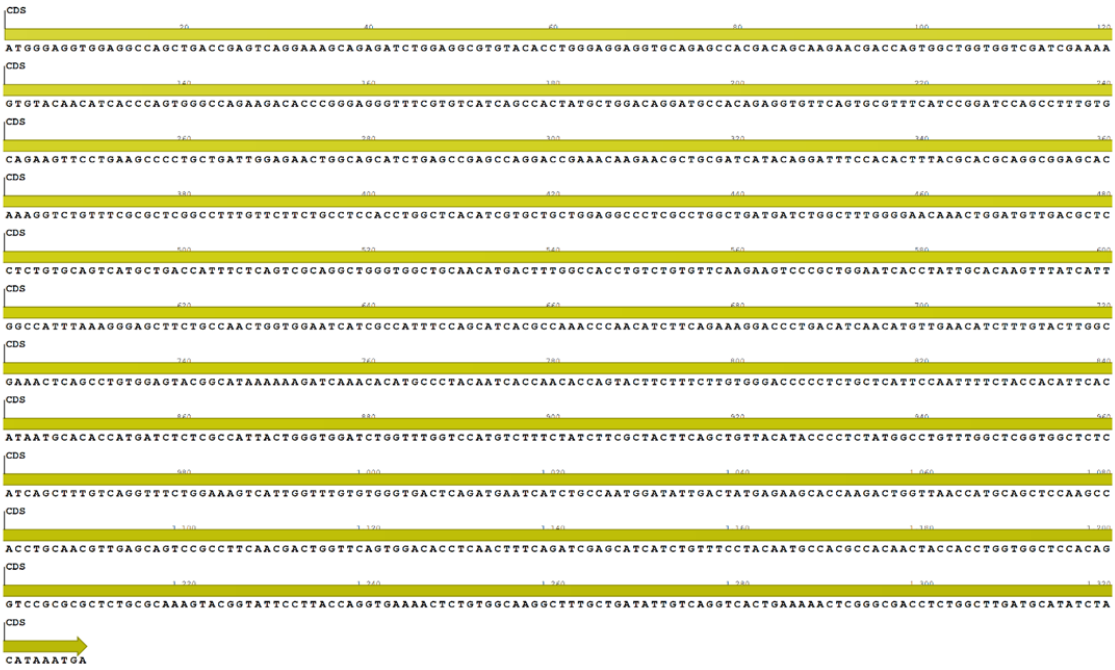

Hypoclinemus mentalis Fads2b amino acid sequence

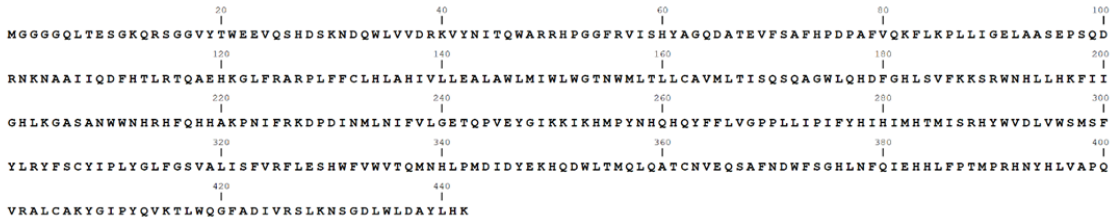

Fig. 36

Hypoclinemus mentalis fads2a and/or *fads2b* mRNA, 5'UTR

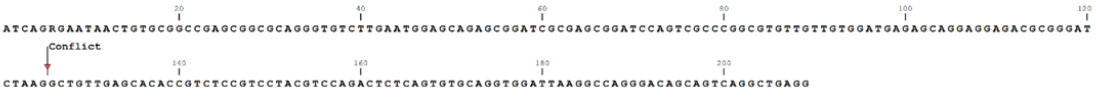

Hypoclinemus mentalis fads2a and/or *fads2b* mRNA, 3'UTR

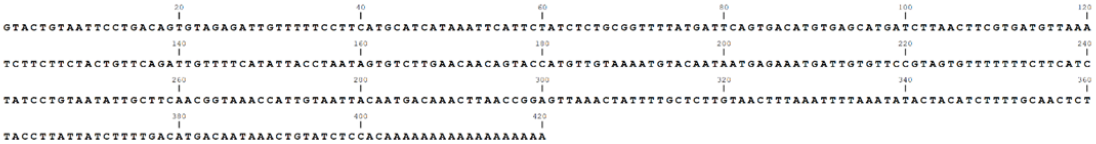

Fig. 37

Gymnachirus melas elovl5 mRNA, partial sequence

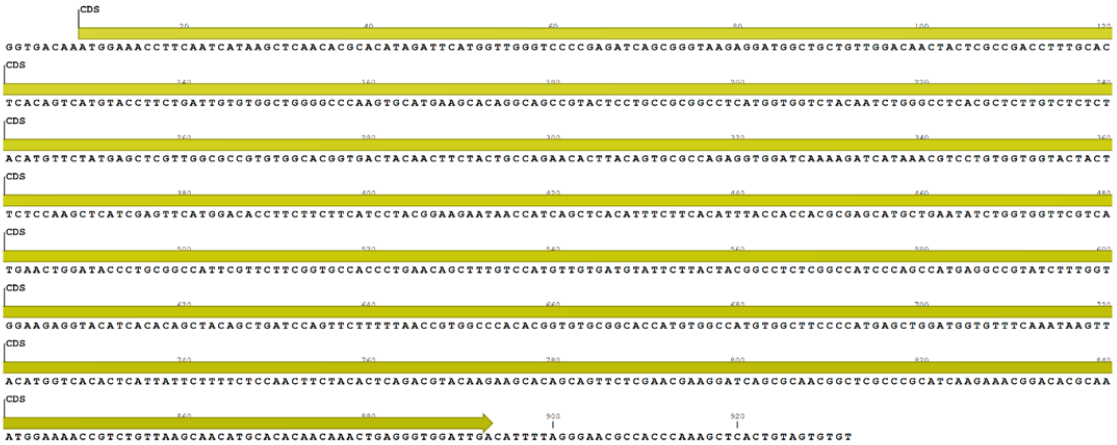

Gymnachirus melas Fads2 amino acid sequence

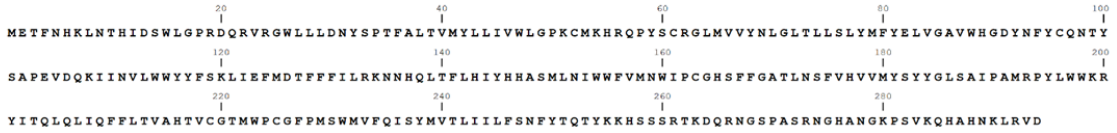

Fig. 38

Trinectes maculatus elovl5 mRNA, complete sequence

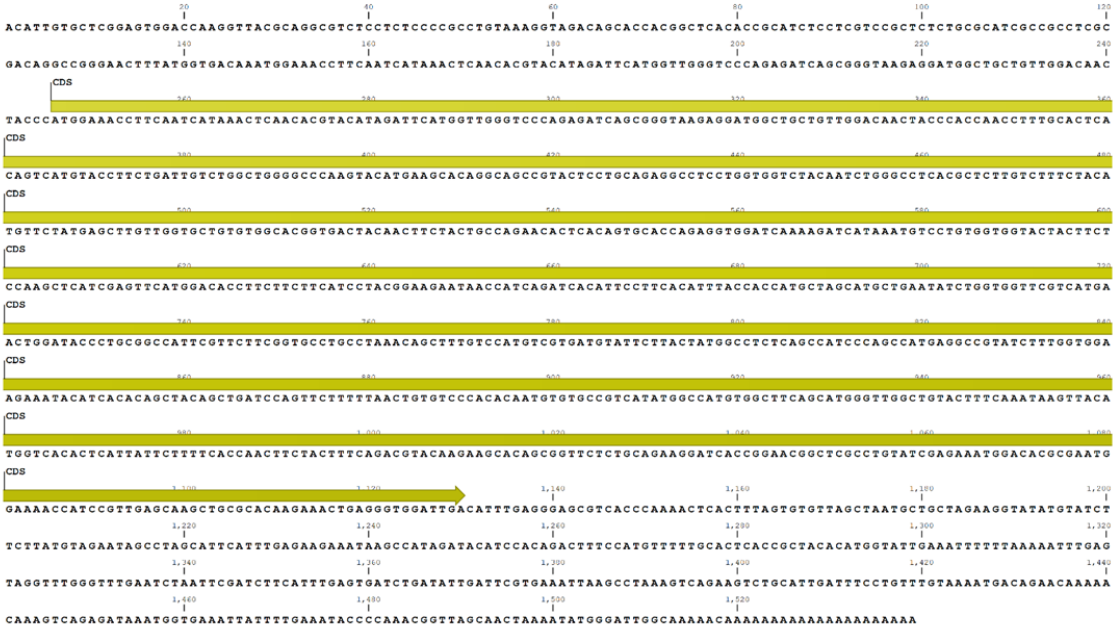

Trinectes maculatus Elovl5 amino acid sequence

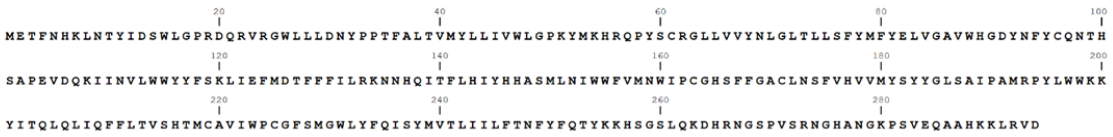

Fig. 39

Apionichthys finis elovl5 mRNA, partial sequence

Apionichthys finis Elovl5 amino acid sequence

Fig. 40

Hypoclinemus mentalis elovl5 mRNA, complete sequence

Hypoclinemus mentalis Elovl5 amino acid sequence

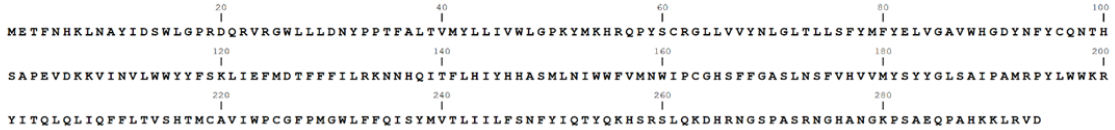

Fig. 41

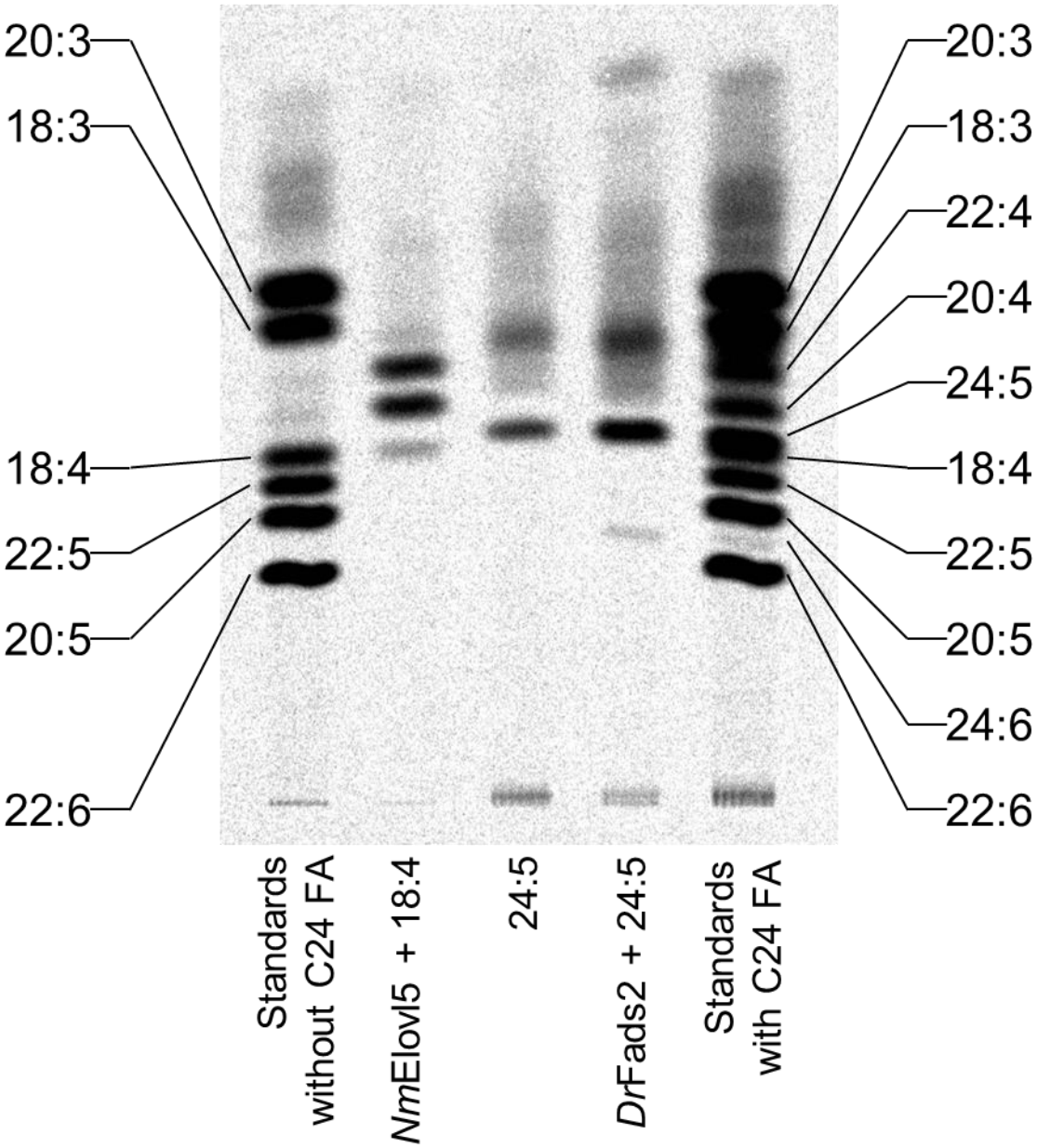
20:3
18:3
18:4
22:5
20:5
22:6
20:3
18:3
22:4
20:4
24:5
18:4
22:5
20:5
24:6
22:6
Standards without C24 FA
NmElovl5 + 18:4
24:5
DrFads2 + 24:5
Standards with C24 FA

Table 1 | Desaturase and elongase activities shown by fatty acid-metabolising enzymes of Achiridae expressed in the recombinant yeast

Supplementary Table 1a. Conversion rates of Elovl5 (%)

Substrate	Product	*G. melas*	*T. maculatus*	*A. finis*	*H. mentalis*	Activity
18:4n–3	20:4n–3	44.8	48.2	37.5	14.9	C18→20
	22:4n–3	31.1	32.8	34.2	60.6	C20→22
	24:4n–3	3.8	3.3	4.5	3.8	C22→24
20:5n–3	22:5n–3	59.5	73.8	62.1	77.6	C20→22
	24:5n–3	23.7	5.4	21.1	11.4	C22→24
22:5n–3	24:5n–3	14.2	3.8	17.7	5.9	C22→24

Supplementary Table 1b. Conversion rates of Fads2 (%)

Substrate	Product	*G. melas*	*T.maculatus*	*A. finis*	*H. mentalis*		Activity
					Fads2a	Fads2b	
18:3n–3	18:4n–3	26.2	39.8	67.6	40.5	1.3	Δ6
20:4n–3	20:5n–3	0.6	6.5	7.3	2.0	2.3	Δ5
22:5n–3	22:6n–3	n.d.	7.2	1.1	n.d.	14.0	Δ4

Supplementary Table 1c. Conversion rates of Fads2 toward 24:5 using co-expression vector (%)

Fads2		Control→Product	24:5n-3→24:6n-3	$\Delta_{24:5n-3}/\Delta_{control}$
G. melas		7.1	4.9	0.7
T. Maculatus		5.3	16.4	3.1
A. finis		6.2	27.8	4.5
H. mentalis	a	6.3	23.4	3.7
	b	n.d.	8.8	-

Supplementary Table 1d. Conversion rates of Fads2 mutants (%)

mutant	18:3n-3→18:4n-3 (Δ6 activity)	22:5n-3→22:6n-3 (Δ4 activity)	Δ4/Δ6
Fads2b V69A	0.7	5.7	8.2
Fads2b L239V	1.1	4.8	4.5
Fads2b Y277F	23.8	2.3	0.1
Fads2b H280Q	3.2	5.6	1.8
Fads2b Y290D	1.3	4.0	3.0
Fads2b F300Y	0.6	1.8	3.1
Fads2b W418S	0.9	4.9	5.3
Fads2b A422T	0.7	4.0	5.7
Fads2a F277Y	2.6	n.d.	-
Fads2a F277Y+Q280H	0.6	1.2	1.9

Table 2. Reference sequences with accession numbers			
Step	**Species**	**Nucleotide**	**Protein**
Determined in this research			
16S rRNA	*Gymnachirus melas*	LC487286	
	Trinectes maculatus	LC487287	
	Apionichthys finis	LC487288	
	Hypoclinemus mentalis	LC487289	
fads2 (CDS)	*Gymnachirus melas*	LC487294	BBL33564
	Trinectes maculatus	LC487295	BBL33565
	Apionichthys finis	LC487296	BBL33566
	Hypoclinemus mentalis	LC487297	BBL33567
		LC487298	BBL33568
fads2 (genomic)	*Hypoclinemus mentalis*	LC490864	
elovl5 (CDS)	*Gymnachirus melas*	LC487290	BBL33560
	Trinectes maculatus	LC487291	BBL33561
	Apionichthys finis	LC487292	BBL33562
	Hypoclinemus mentalis	LC487293	BBL33563
Phylogenetic analysis			
16S rRNA	*Citharoides macrolepidotus*	AP014588	
	Lepidoblepharon ophthalmolepis	KJ433560	
fads1	*Callorhinchus milii*	XM_007887444	XP_007885635
	Scyliorhinus canicula	JN657543	AEY94454
fads2	*Callorhinchus milii*	XM_007887445	XP_007885636
	Scyliorhinus canicula	JN657544	AEY94455
	Salmo salar	AF478472	AAL82631
		AY458652	AAR21624
		GU207400	ADA56788
		GU207401	ADA56789
	Siganus canaliculatus	EF424276	ABR12315
		GU594278	GU594278
	Oreochromis niloticus	KF268464	ADJ29913
		XM_003440472	XP_003440520
	Chirostoma estor	KJ417838	AHX39206
		KJ417839	AHX39207
	Channa striata	EU570220	ACD70298
		KT962985	AMY15661
	Danio rerio	AF309556	AAG25710
	Solea senegalensis	JN673546	AEQ92868
	Clarias gariepinus	KU925904	AMR43366
	Oryzias latipes	XM_011476059	XP_011474361
	Lates calcarifer	GQ214179	ACS91458
	Rachycentron canadum	FJ440238	ACJ65149
	Scophthalmus maximus	AY546094	AAS49163
	Paralichthys olivaceus	KM893456	AJG36440
	Gadus morhua	DQ054840	AAY46796
	Sparus aurata	GQ162822	ADD50000
	Nibea mitsukurii	GQ996729	ACX54437

Table 2. Reference sequences with accession numbers (continued)			
Step	**Species**	**Nucleotide**	**Protein**
Designing degenerate primers			
16S rRNA	*Achirus lineatus*	JQ939049	
	Gymnachirus melas	JQ939050	
	Gymnachirus texae	JQ939051	
	Trinectes maculatus	JQ939052	
fads2	*Scophthalmus maximus*	AY546094	AAS49163
	Solea senegalensis	JN673546	AEQ92868
	Paralichthys olivaceus	KM893456	AJG36440
	Cynoglossus semilaevis	XM_008312161	XP_008310383
elovl5	*Scophthalmus maximus*	AF465520	AAL69984
	Solea senegalensis	JN793448	AER58183
	Paralichthys olivaceus	KM893457	AJG36441
	Cynoglossus semilaevis	XM_008322048	XM_008322048

Table 3. Primers used in this study		
Step	**Primer name**	**Sequence (5' to 3')**
cDNA synthesis	oligo_dT_adapter_primer	GTAATACGACTCACTATAGGGCACGCGTGGTC-
		GACGGCCCGGGCTGGTTTTTTTTTTTTTTTT
Phylogenetic analysis	16S_Fw	CATCTCTGTGGCAAAAGAGT
	16S_Rv	TAGGATGTCCTGATCCAACAT
Degenerate PCR	flatfish_fads2_F1	TGGRARGAGGTGCARARMCACAGCA
	flatfish_fads2_F2	AAAAGACAYCCAGGAGGGTTTC
	flatfish_fads2_R1	AGATGATGYTCGATYTGAAAGTTGAG
	flatfish_fads2_R2	AGCTGCATKGTTAACCAGTCCT
	flatfish_elovl5_F1	CACCAACCTTTGCACTCACA
	flatfish_elovl5_F2	CTTCTGATTGTGTGGATGGG
	flatfish_elovl5_R1	TCTTGTACGTCTGAATGTAG
	flatfish_elovl5_R2	GCTGWAACTGTGTGATGTAT
RACE	3'RACE_adapter_R1	CCATCCTAATACGACTCACTATAGGGC
	3'RACE_adapter_Rn	CTATAGGGCACGCGTGGT
	Hm_fads2_5'RACE_R1	AGGTGGAGGCAGAAGAACAA
	Hm_fads2_5'RACE_Rn	GTTCTTGTTTCGGTCCTGGCT
	Hm_fads2_3'RACE_F1	CCCCCTCTGCTCATTCCAATTT
	Hm_fads2_3'RACE_Fn	CTGGGTGGATCTGGTTTGGT
	Tm_fads2_5'RACE_R1	CTGGATCCGGATGAAAAGCAGAAAACAC
	Tm_fads2_5'RACE_Rn	AGCATAGTGGGCGATGACACGGAAG
	Tm_fads2_3'RACE_F1	GGTGTGTTTGGCTCGTTGGCTCT
	Tm_fads2_3'RACE_Fn	TGGAAAGTCACTGGTTTGTGTGGG
	Hm_elovl5_5'RACE_R1	TGTGAGTGTTTTGGCAGTAGAAGTT
	Hm_elovl5_5'RACE_Rn	CCACACAGCACCCACAAGCTCAT
	Hm_elovl5_3'RACE_F1	GAGGCCGTATCTTTGGTGGAA
	Hm_elovl5_3'RACE_Fn	AGATACATCACACAGCTACAG
	Tm_elovl5_5'RACE_R1	ATGTAGAAAGACAAGAGCGTGAGG
	Tm_elovl5_5'RACE_Rn	CCCCAGCCAGACAATCAGAAGGTACAT
	Tm_elovl5_3'RACE_F1	TTCGTTCTTCGGTGCCTGCCTA
	Tm_elovl5_3'RACE_Fn	TGTGGCTTCAGCATGGGTTGG
CDS cloning	Hm_fads2_5'UTR_Fw	TGTTGTTGTGGATGAGAG
	Hm_fads2_3'UTR_Rv	AACCGCAGAGATAGAATGA
	Hm_Tm_elovl5_5'UTR_Fw	CAGGCTGGCAACTTTATGGT
	Hm_Tm_elovl5_3'UTR_Rv	AGCATCATTAGCTAACACAC
	Tm_fads2_5'UTR_Fw	GTTGTTGTGGATGAGAGCTGGA
	Tm_fads2_3'UTR_Rv	TTTTATGGCTGGTGCGACTTGT
	Achiridae_fads2_5'UTR_F1	AGTGTGCAGGTGGATTAAGG
	Achiridae_fads2_5'UTR_F2	GGATTAAGGCCAGGGACAGC
	Achiridae_fads2_3'UTR_R1	GAATCATAAAACYGSAGAGA
	Achiridae_fads2_3'UTR_R2	ACYGSAGAGATAGAATKAAT
	Achiridae_elovl5_5'UTR_F1	CGMCAGGCYGGSAACTTTAT
	Achiridae_elovl5_5'UTR_F2	GGCYGGSAACTTTATGGTGACAAA
	Achiridae_elovl5_3'UTR_R1	AGCAKCATTAGCTAACACACT
	Achiridae_elovl5_3'UTR_R2	ACTAMAGTGARYTTTGGGTGACG

Table 3. Primers used in this study (continued)		
Step	**Primer name**	**Sequence (5' to 3')**
Vector construction	Hm_Af_Fads2_Fw_HindIII	ATTAAGCTTGAGATGGGAGGTGGAGGCCAGCTGA
	Hm_Af_Fads2_Rv_XbaI	AGTTCTAGATCATTTATGTAGATATGCATCAA
	Tm_Fads2_Fw_HindIII	AAAAAGCTTAGGATGGGAGGTGGAGGCCAGTTGAC
	Tm_Fads2_Rv_XbaI	CCCTCTAGATCATTTATGTAGATACGCATCAAGCC
	Gm_Fads2_Fw_HindIII	AAAAAGCTTAGGATGGGAGGTGGAGGCCAGCGGTC
	Gm_Fads2_Rv_XbaI	CCCTCTAGATCATTTATGTAAATATGCATCGAGCC
	Hm_Tm_Elovl5_Fw_HindIII	ATCAAGCTTAAAATGGAAACCTTCAATCATAAACTCAA
	Hm_Elovl5_Rv_XbaI	ATTTCTAGATCAATCCACCCTCAGTTTCTTGTGT
	Tm_Elovl5_Rv_XbaI	TAATCTAGATCAATCCACCCTCAGTTTCTTGTGCG
	Af_Elovl5_Fw_HindIII	GGGAAGCTTAAAATGGAAACCGTCAATCATAAATT
	Af_Elovl5_Rv_XbaI	TTTTCTAGATCAATCCACCCTCAGTTTCTTGTGTG
	Dr_Fads2_Fw_HindIII	ACGAAGCTTACGATGGGTGGCGGAGGACAGCAGACA
	Dr_Fads2_Rv_XbaI	ACGTCTAGATTATTTGTTGAGATACGCATCCA
	Dr_Elovl2_Fw_KpnI	CCGGGTACCAATATGGAATCATATGAAAA
	Dr_Elovl2_Rv_XbaI	CGGTCTAGATCACTGTAGCTTCTGTTTGG
	pYES2_linearize_Fw	TCCACAGAATCAGGGGATAAC
	pYES2_linearize_Rv	TAACCGTATTACCGCCTTTGAGT
	PADH1_DrElovl2_TADH1_Fw	GCGGTAATACGGTTATCTAGCTCCCTAACATGT
	PADH1_DrElovl2_TADH1_Rv	CCCTGATTCTGTGGAGTGTGGAAGAACGATTAC
Genomic analysis	Hm_gfads2_5'Fw	AAAAGTGTACAACATCACCC
	Hm_gfads2_5'Rv	ATCTCTGCTTTCCTGACTCG
	Hm_gfads2_3'Fw	CTCTGGCTTGATGCATATCT
	Hm_gfads2_3'Rv	CCCGAGTTTTTCAGTGACCT
Mutagenesis	Hm_Fads2b_V69A_Fw	ACAGAGGCGTTCAGTGCGTTTCATCCGGATCCA
	Hm_Fads2b_V69A_Rv	ACTGAACGCCTCTGTGGCATCCTGTCCAGCATA
	Hm_Fads2b_L239V_Fw	CTTTGTAGTTGGCGAAACTCAGCCTGTGGAGTA
	Hm_Fads2b_L239V_Rv	TCGCCAACTACAAAGATGTTCAACATGTTGATG
	Hm_Fads2b_Y277F_Fw	ATTTTCTTCCACATTCACATAATGCACACCATG
	Hm_Fads2b_Y277F_Rv	AATGTGGAAGAAAATTGGAATGAGCAGAGGGGG
	Hm_Fads2b_H280Q_Fw	ACATTCAGATAATGCACACCATGATCTCTCGCC
	Hm_Fads2b_H280Q_Rv	GCATTATCTGAATGTGGTAGAAAATTGGAATGA
	Hm_Fads2b_Y290D_Fw	TCGCCATGACTGGGTGGATCTGGTTTGGTCCAT
	Hm_Fads2b_Y290D_Rv	ACCCAGTCATGGCGAGAGATCATGGTGTGCATT
	Hm_Fads2b_F300Y_Fw	ATGTCTTACTATCTTCGCTACTTCAGCTGTTAC
	Hm_Fads2b_F300Y_Rv	AAGATAGTAAGACATGGACCAAACCAGATCCAC
	Hm_Fads2b_W418S_Fw	ACTCTGTCGCAAGGCTTTGCTGATATTGTCAGG
	Hm_Fads2b_W418S_Rv	GCCTTGCGACAGAGTTTTCACCTGGTAAGGAAT
	Hm_Fads2b_A422T_Fw	AGGCTTTACTGATATTGTCAGGTCACTGAAAAA
	Hm_Fads2b_A422T_Rv	ATATCAGTAAAGCCTTGCCACAGAGTTTTCACC
	Hm_Fads2a_F277Y_Fw	ATTTTCTACCACATTCAGATAATGCACACCATG
	Hm_Fads2a_F277Y_Rv	AATGTGGTAGAAAATTGGAATGAGCAGAGGGGG
	Hm_Fads2a_F277Y+Q280H_Fw	TTTTCTACCACATTCACATAATGCACACCATGATC
	Hm_Fads2a_F277Y+Q280H_Rv	CATTATGTGAATGTGGTAGAAAATTGGAATGAGCA

Table 4. PCR conditions

				Denature tenperature (°C)	Annealing tremprature (°C)	Extention temperature (°C)	Number of cycles
PCR	**Forward primer**	**Reverse primer**	**DNA polymerase**	**(duration in s)**	**(duration in s)**	**(duration in s)**	
Achiridae							
16S rRNA gene	16S_Fw	16S_Rv	PrimeSTAR Max DNA Polymerase	98 (10)	55 (5)	72 (20)	35
H. mentalis							
fads2 cloning							
Degenerate PCR	flatfish_fads2_F1	flatfish_fads2_R1	TaKaRa Ex Taq	94 (30)	58 (30)	72 (60)	35
5'RACE 1st PCR	GeneRacer 5'	Hm_fads2_5'RACE_R1	TaKaRa Ex Taq	94 (30)	72 > 57 (35)*	72 (60)	35
5'RCAE nested PCR	GeneRacer 5' nested	Hm_fads2_5'RACE_Rn	TaKaRa Ex Taq	94 (30)	55 (30)	72 (60)	30
3'RACE 1st PCR	Hm_fads2_3'RACE_F1	3'RACE_adapter_R1	TaKaRa Ex Taq	94 (30)	72 > 57 (35)*	72 (60)	35
3'RACE nested PCR	Hm_fads2_3'RACE_Fn	3'RACE_adapter_Rn	TaKaRa Ex Taq	94 (30)	55 (30)	72 (60)	30
CDS cloning	Hm_fads2_5'UTR_Fw	Hm_fads2_5'UTR_Rv	PrimeSTAR Max DNA Polymerase	98 (10)	55 (5)	72 (20)	35
Vector construction	Hm_Af_Fads2_Fw_HindIII	Hm_Af_Fads2_Rv_XbaI	PrimeSTAR Max DNA Polymerase	98 (10)	55 (5)	72 (20)	35
elovl5 cloning							
Degenerate PCR	flatfish_elovl5_F2	flatfish_elovl5_R1	TaKaRa Ex Taq	94 (30)	52 (30)	72 (60)	35
5'RACE 1st PCR	GeneRacer 5'	Hm_elovl5_5'RACE_R1	TaKaRa Ex Taq	94 (30)	70 > 55 (35)*	72 (90)	35
5'RACE nested PCR	GeneRacer 5' nested	Hm_elovl5_5'RACE_Rn	TaKaRa Ex Taq	94 (30)	58 (30)	72 (90)	35
3'RACE 1st PCR	Hm_elovl5_3'RACE_F1	3'RACE_adapter_R1	TaKaRa Ex Taq	94 (30)	70 > 55 (35)*	72 (90)	35
3'RACE nested PCR	Hm_elovl5_3'RACE_Fn	3'RACE_adapter_Rn	TaKaRa Ex Taq	94 (30)	58 (30)	72 (90)	35
CDS cloning	Hm_elovl5_5'UTR_Fw	Hm_elovl5_3'UTR_Rv	PrimeSTAR Max DNA Polymerase	98 (10)	55 (5)	72 (20)	35
Vector construction	Hm_Elovl5_Fw_HindIII	Hm_Elovl5_Rv_XbaI	PrimeSTAR Max DNA Polymerase	98 (10)	55 (5)	72 (20)	35
Genomic fads2 analysis	Combinations of primer series		TaKaRa LA Taq	94 (10)	68 (900)**		30
	for genomic analysis		PrimeSTAR GXL DNA Polymerase	98 (10)	60 (15)	68 (10)	30
fads2 mutagenesis	Each pair of primer series		PrimeSTAR Max DNA Polymerase	98 (10)	55 (15)	72 (40)	30
	for mutagenesis						
T. maculatus							
fads2 cloning							
Degenerate PCR	flatfish_fads2_F1	flatfish_fads2_R1	TaKaRa Ex Taq	94 (30)	55 (30)	72 (60)	35
5'RACE 1st PCR	GeneRacer 5'	Tm_fads2_5'RACE_R1	PrimeSTAR HS DNA Polymerase	98 (10)	55 (5)	72 (60)	30
5'RCAE nested PCR	GeneRacer 5' nested	Tm_fads2_5'RACE_Rn	PrimeSTAR HS DNA Polymerase	98 (10)	55 (5)	72 (60)	30
3'RACE 1st PCR	Tm_fads2_3'RACE_F1	3'RACE_adapter_R1	PrimeSTAR HS DNA Polymerase	98 (10)	55 (5)	72 (60)	30
3'RACE nested PCR	Tm_fads2_3'RACE_Fn	3'RACE_adapter_Rn	Tks Gflex DNA Polymerase	98 (10)	60 (15)	68 (30)	30
CDS cloning	Tm_fads2_5'UTR_Fw	Tm_fads2_5'UTR_Rv	PrimeSTAR Max DNA Polymerase	98 (10)	55 (5)	72 (20)	35
Vector construction	Tm_Fads2_Fw_HindIII	Tm_Fads2_Rv_XbaI	PrimeSTAR Max DNA Polymerase	98 (10)	55 (5)	72 (20)	35
elovl5 cloning							
Degenerate PCR	flatfish_elovl5_F1	flatfish_elovl5_R1	TaKaRa Ex Taq	94 (30)	55 (30)	72 (60)	35
5'RACE 1st PCR	GeneRacer 5'	Tm_elovl5_5'RACE_R1	TaKaRa Ex Taq	94 (30)	72 > 57 (35)*	72 (90)	35
5'RCAE nested PCR	GeneRacer 5' nested	Tm_elovl5_5'RACE_Rn	TaKaRa Ex Taq	94 (30)	72 > 57 (35)*	72 (90)	35
3'RACE 1st PCR	Tm_elovl5_3'RACE_F1	3'RACE_adapter_R1	TaKaRa Ex Taq	94 (30)	72 > 57 (35)*	72 (90)	35
3'RACE nested PCR	Tm_elovl5_3'RACE_Fn	3'RACE_adapter_Rn	TaKaRa Ex Taq	94 (30)	60 (30)	72 (90)	35
CDS cloning	Hm_Tm_elovl5_5'UTR_Fw	Hm_Tm_elovl5_5'UTR_Fw	PrimeSTAR Max DNA Polymerase	98 (10)	55 (5)	72 (20)	35
Vector construction	Hm_Tm_Elovl5_Fw_HindIII	Tm_Elovl5_Rv_XbaI	PrimeSTAR Max DNA Polymerase	98 (10)	55 (5)	72 (20)	35

Table 4. PCR conditions (continued)

				Denature tenperature (°C)	Annealing tremprature (°C)	Extention temperature (°C)	Number of cycles
PCR	**Forward primer**	**Reverse primer**	**DNA polymerase**	**(duration in s)**	**(duration in s)**	**(duration in s)**	
A. finis							
fads2 cloning							
CDS cloning	Achiridae_fads2_5'UTR_F1	Achiridae_fads2_3'UTR_R1	PrimeSTAR Max DNA Polymerase	98 (10)	55 (5)	72 (20)	35
Vector construction	Hm_Af_Fads2_Fw_HindIII	Hm_Af_Fads2_Rv_XbaI	PrimeSTAR Max DNA Polymerase	98 (10)	55 (5)	72 (20)	35
elovl5 cloning							
CDS cloning	Achiridae_elovl5_5'UTR_F1	Achiridae_elovl5_3'UTR_R1	PrimeSTAR Max DNA Polymerase	98 (10)	55 (5)	72 (20)	35
Vector construction	Af_Elovl5_Fw_HindIII	Af_Elovl5_Rv_XbaI	PrimeSTAR Max DNA Polymerase	98 (10)	55 (5)	72 (10)	30
G. melas							
fads2 cloning							
CDS cloning	Achiridae_fads2_5'UTR_F2	Achiridae_fads2_3'UTR_R1	PrimeSTAR Max DNA Polymerase	98 (10)	55 (5)	72 (10)	30
Vector construction	Gm_Fads2_Fw_HindIII	Gm_Fads2_Rv_XbaI	PrimeSTAR Max DNA Polymerase	98 (10)	55 (5)	72 (10)	30
elovl5 cloning							
CDS cloning	Achiridae_elovl5_5'UTR_F1	Achiridae_elovl5_3'UTR_R1	PrimeSTAR Max DNA Polymerase	98 (10)	55 (5)	72 (10)	30
Vector construction	Gm_Elovl5_Fw_HindIII	Gm_Elovl5_Rv_XbaI	PrimeSTAR Max DNA Polymerase	98 (10)	55 (5)	72 (10)	30
D. rerio							
fads2 vector construction	Dr_Fads2_Fw_HindIII	Dr_Fads2_Rv_XbaI	PrimeSTAR Max DNA Polymerase	98 (10)	55 (5)	72 (10)	30
elovl2 vector construction	Dr_Elovl2_Fw_KpnI	Dr_Elovl2_Rv_XbaI	PrimeSTAR Max DNA Polymerase	98 (10)	55 (5)	72 (10)	30
Constructing co-expression vectors							
Linearizing pYES2	pYES2_linearize_Fw	pYES2_linearize_Rv	PrimeSTAR Max DNA Polymerase	98 (10)	55 (5)	72 (40)	30
Isolating ADH1-elovl2	PADH1_DrElovl2_TADH1_Fw	PADH1_DrElovl2_TADH1Rv	PrimeSTAR Max DNA Polymerase	98 (10)	55 (5)	72 (10)	30

謝辞

本研究の遂行および論文の作成をはじめ、研究生活のありとあらゆることについて、終始温かく丁寧なご指導、ご鞭撻、およびご校閲を賜りました東京海洋大学海洋生命科学部海洋生物資源学科水族生理学研究室教授　吉崎　悟朗博士に心より感謝の意を表します。

本論文のご校閲を賜り、有益なご教示を下さった東京海洋大学海洋生命科学部海洋生物資源学科水族生理学研究室准教授　矢澤　良輔博士、同水族栄養学研究室教授　佐藤　秀一博士に謝意を表します。

博士前期課程から新たな課題に取り組むにあたり、ひとつひとつ丁寧にご指導下さり、先達として常に明るく道を照らして下さった、東京海洋大学海洋生命科学部海洋生物資源学科水族栄養学研究室助教　壁谷　尚樹博士に深く感謝の意を表します。

本研究において耳石の分析をご担当いただいた水産研究・教育機構水産技術研究所　三好　花歩博士、アキルス科海産種 *Gymnachirus melas* の貴重な生体サンプルの入手に尽力下さったアメリカ海洋大気庁 John Adam Luckenbach 博士、論文投稿の際に丁寧なご校閲を賜りました東京海洋大学海洋科学部海洋資源学科集団生物学研究室の　ストルスマン　カルロス　アウグスト博士に感謝の意を表します。

研究遂行にあたり、適切なご助言を頂いたうえ、実験設備を快くご貸与下さった集団生物学研究室准教授　山本　洋嗣博士、水族栄養学研究室准教授　芳賀　穣博士、同学放射性同位元素管理センター　伊藤　友加里様に厚く御礼申し上げます。

また、水族生理学研究室における研究生活を支えて下さいました卒業生の皆様、研究員の皆様、職員の皆様に心から感謝の意を表します。

最後に、研究遂行のため犠牲となった数多くの実験魚の命に対し、感謝と慰霊の念を謹んで捧げます。